

1 **Comparing Model Representations of Physiological Limits on Transpiration**
2 **at a Semi-arid Ponderosa Pine Site**

3
4 Linnia R. Hawkins¹, Maoya Bassouni², William R. L. Anderegg³, Martin D. Venturas⁴, Stephen
5 P. Good⁵, Hyojung J. Kwon¹, Chad V. Hanson¹, Richard P. Fiorella⁶, Gabriel J. Bowen⁶, and
6 Christopher J. Still¹

7
8 ¹Department of Forestry, Oregon State University, Corvallis, OR

9 ²Department of Crop Production Ecology, Swedish University of Agricultural Sciences, Uppsala,
10 Sweden

11 ³School of Biological Sciences, University of Utah, Salt Lake, UT

12 ⁴Departamento de Sistemas y Recursos Naturales, Universidad Politécnica de Madrid, Madrid,
13 Spain

14 ⁵Department of Biological and Ecological Engineering, Oregon State University, Corvallis, OR

15 ⁶Department of Geology and Geophysics, University of Utah, Salt Lake, UT

16
17 Corresponding author: Linnia Hawkins (Linnia.Hawkins@oregonstate.edu)

18
19 **Key Points:**

- 20 • We evaluate several model formulations for coupling plant hydraulic and stomatal
21 functioning using functional performance metrics.
- 22
- 23 • Information flows from soil water potential and vapor pressure deficit to transpiration
24 illustrate functional differences among models.
- 25
- 26 • Considerable biases in modeled canopy temperature propagate to a 5% offset in
27 cumulative growing season transpiration.

28 **Abstract**

29

30 Mechanistic representations of biogeochemical processes in ecosystem models are rapidly
31 advancing, requiring advancements in model evaluation approaches. Here we quantify multiple
32 aspects of model functional performance to evaluate improved process representations in
33 ecosystem models. We compare semi-empirical stomatal models with hydraulic constraints
34 against more mechanistic representations of stomatal and hydraulic functioning at a semi-arid
35 pine site using a suite of metrics and analytical tools. We find that models generally perform
36 similarly under unstressed conditions, but performance diverges under atmospheric and soil
37 drought. The more empirical models better capture synergistic information flows between soil
38 water potential and vapor pressure deficit to transpiration, while the more mechanistic models
39 are overly deterministic. Additionally, both multilayer canopy and big-leaf models were unable
40 to capture the magnitude of canopy temperature divergence from air temperature. Lastly,
41 modeled stable carbon isotope fractionation differed under canopy water stress which illustrates
42 the value of carbon isotopes in helping to characterize ecosystem function and elucidate
43 differences attributable to model structure. This study demonstrates the value of merging
44 underutilized observational data streams with emerging analytical tools to characterize
45 ecosystem function and discriminate among model process representations.

46

47 **Plain Language Summary**

48

49 Earth system models are an essential tool for understanding the consequences of changing
50 climate conditions on forest ecosystems. Models are rapidly incorporating more realistic
51 representations of how drought impacts ecosystem carbon and water cycling. These
52 advancements need to be thoroughly evaluated to ensure that the models adequately capture the
53 plant functional response to drought stress. Here we merge underutilized measurements with new
54 analytical tools to evaluate several model representations of plant response to drought. These
55 tools allow us to both better understand relationships among drought stress and ecosystem
56 response, as well as quantify model accuracy. We find that models generally perform similarly
57 under unstressed conditions, but performance diverges under atmospheric and soil drought.

58

59 **1 Introduction**

60

61 Climate change mitigation, adaptation, and conservation efforts all leverage ecosystem models to
62 understand and predict carbon and water cycling at local to global scales. Ecosystem models
63 have rapidly advanced in recent decades and now incorporate mechanistic representations of
64 many plant and soil processes (e.g., Kennedy et al., 2019; Sabot et al., 2020; Eller et al., 2020).
65 Recent developments have focused on the representation of plant hydraulic functioning to
66 improve mechanistic modeling of water transport through the soil-plant-atmosphere continuum,
67 but how best to represent the effects of drought stress on plant gas-exchange, especially when
68 quantifying ecosystem-scale fluxes, is still an open question (Mencuccini et al., 2019).
69 Evaluating improved plant hydraulic representation in ecosystem models requires more
70 comprehensive frameworks for quantifying model performance, including both metrics for
71 evaluating functional relations among processes, and comparisons against underutilized
72 observational data.

73 Early land surface models (e.g., Bonan et al., 1995; Cox et al., 1998) implemented an empirical
74 model for stomatal functioning based on gas-exchange measurements (Ball et al., 1987), which
75 has been used for decades with strong empirical support (e.g., Damour et al., 2010; Lin et al.,
76 2015). However, a predominant theory of stomatal functioning (Cowan and Farquhar, 1977)
77 assumes plants optimize stomatal behavior such that the benefit of carbon gained (A) is
78 equivalent to the respective cost of water loss by way of transpiration (T). As such, stomata
79 optimize the tradeoff between carbon gain and the carbon cost of transpiration, $A - \lambda T$, where λ
80 ($\text{mol CO}_2 / \text{mol H}_2\text{O}$) is the carbon cost per unit water used by the plant. This theoretical basis
81 has been used to develop semi-empirical stomatal models (Medlyn et al., 2011), which have been
82 shown to be fundamentally based on the same physiological principles as the Ball et al., (1987)
83 model (Franks et al., 2017).

84 Many studies have demonstrated that semi-empirical models perform well under well-watered
85 conditions but do not capture soil drought responses correctly (e.g. Powell et al., 2013; Bonan et
86 al., 2014; Medlyn et al., 2016; Ukkola et al., 2016). These semi-empirical models are limited by
87 the need to prescribe a constant value for λ , which does not respond to environmental conditions
88 and is not based on measurable plant traits (Buckley, 2017). Optimization theory supports the

89 conceptual framework of hydraulic limitation on gas exchange since the cost of hydraulic
90 damage can be incorporated into the cost of water loss. However, there is little consensus on how
91 best to represent hydraulic costs in models.

92 To directly couple stomatal conductance to plant hydraulic mechanisms, model formulations of
93 optimal stomatal behavior have been proposed that assume plants balance carbon gain against
94 hydraulic risk (e.g. Williams et al., 1996; Sperry et al., 2017; Mencuccini et al., 2019; Wang et
95 al., 2020). The mechanistic optimization models have the advantage of being parameterized with
96 measurable plant traits and have been shown to perform well at the plant scale (e.g., Venturas et
97 al., 2018; Wang et al., 2020). A comparison of different stomatal optimization principles in a
98 big-leaf framework, indicated that formulations with explicit representation of plant hydraulics
99 did not substantially improve ecosystem-scale evapotranspiration estimates (Bassiouni and Vico,
100 2021). At the ecosystem scale, Sabot et al., (2020) found that the Sperry et al., (2017) model
101 demonstrated improved performance over the Medlyn et al., (2011) model and Bonan et al.,
102 (2014) showed that the Soil-Plant-Atmosphere optimization model (Williams et al., 1996)
103 demonstrated some improvement over the Ball et al., (1987) model when water availability was
104 limited. However, both evaluations only compared the more mechanistic models against semi-
105 empirical models without hydraulic constraints. Although there is still much discussion about
106 how hydraulic functioning should be applied in semi-empirical models (Lin et al., 2015),
107 hydraulic limitations have been incorporated into semi-empirical stomatal models (Tuzet et al.,
108 2003; Zhou et al., 2013; Wolf et al., 2016; Xu et al., 2016; Yang et al., 2019; Kennedy et al.,
109 2019).

110 Here we compare semi-empirical models with hydraulic constraints against more mechanistic
111 optimization models at the ecosystem scale. We implement hydraulic constraints within the Ball
112 et al., (1987) and Medlyn et al., (2011) models by altering the water use efficiency parameter as
113 a function of the leaf water potential. We evaluate these hydraulic-modified semi-empirical
114 models against two mechanistic approaches. One approach was developed by Williams et al.,
115 (1996) in the soil-plant-atmosphere model (SPA) where the stomatal conductance is calculated to
116 optimize water-use efficiency while avoiding hydraulic failure. This model conceptualizes
117 hydraulic failure by a simple minimum leaf water potential threshold. Another approach we
118 evaluate here is the Sperry et al., (2017) model of optimal stomatal behavior which assumes

119 plants maximize carbon gain while avoiding hydraulic risk. This model integrates across xylem
120 elements to determine the hydraulic vulnerability at an instantaneous drop in canopy water
121 potential.

122 Model intercomparisons are commonly performed by benchmarking the mean state and
123 variability of simulated carbon and water fluxes against observations (e.g. Kennedy et al., 2019;
124 Sabot et al., 2020). But it is particularly important to ensure that the functional relationships
125 among environmental conditions and ecosystem responses are also adequately captured
126 (Kirchner, 2006; Ruddell et al., 2019; Bassiouni & Vico, 2021), particularly when models are
127 intended to make future projections. We leverage ecosystem-scale measurements from a long
128 running intensively monitored AmeriFlux core site in a seasonally drought stressed ecosystem
129 and employ a suite of diagnostics designed to disentangle physiological limits on transpiration.
130 We evaluate the influence of different model process representations on the simulated functional
131 relationships among meteorological conditions, soil water availability, and transpiration at
132 diurnal to daily time scales and for a range of atmospheric and/or soil water stressed conditions.
133 This study demonstrates the value of merging observational data and novel analytical tools to
134 characterize ecosystem function and discriminate among model representations.

135

136 **2 Methods**

137

138 *2.1 Site and observational data description*

139

140 The Metolius forest study site is in a mature coniferous forest in central Oregon at an elevation
141 of 1253 m asl. The forest is a core research site in the AmeriFlux network (site US-Me2) where
142 microclimate and eddy-covariance flux measurements are collected from a flux tower. The
143 canopy is dominated by ponderosa pine trees (*Pinus ponderosa*) with scattered incense cedars
144 (*Calocedrus decurrens*). Trees are evenly distributed with a leaf area index (LAI) of 2.8 (m² leaf
145 m⁻² ground). Tree height is relatively homogeneous at about 18 m, and the mean tree density is
146 approximately 339 trees ha⁻¹ (Irvine et al., 2008). The climate is semi-arid, with warm and dry
147 summers and cool and wet winters, with most precipitation occurring as snow or rain during the
148 winter and spring (November through April). Additional descriptions of the study site, as well as
149 information on site instrumentation and measurements, can be found in Law et al. (2001), Irvine

150 et al., (2004), Thomas et al., (2009) and Ruehr et al., (2014). In this study, we examine the period
151 of 2006-01-01 to 2018-12-31 where the observational records of data streams overlap. We define
152 the growing season as May 1st to August 31st which coincides with the warmest and driest
153 months of the year at this site.

154

155 The US-Me2 site is instrumented with a 33m tower measuring above canopy eddy-covariance
156 fluxes of CO₂, H₂O, latent and sensible heat. Mature ponderosas have been instrumented with
157 sapflow probes which are used to estimate whole tree transpiration by scaling with estimates of
158 sapwood area (see Kwon et al., 2018). We also calculate the canopy conductance per unit ground
159 area (G_c , mm/s) from the sapflow estimates of transpiration, air temperature (T_a , °C), and vapor
160 pressure deficit (VPD, kPa) using a simplified form of the Penman-Monteith equation as
161 suggested by Monteith and Unsworth (1990) as is typically used in ecohydrological studies
162 (Kwon et al., 2018). Canopy temperature was also measured in 2015 (Kim et al., 2016) using a
163 thermal camera (FLIR A325sc). The thermal camera measured the temperature of the upper
164 canopy and we averaged over a selected area of interest to represent only canopy foliage. Soil
165 probes measure soil water content at 10, 20, 30, 50, 70, 100, 130, 160cm depths (Sentek
166 Technologies, Stepney, SA, Australia). We calculated the root weighted soil water potential
167 using the relationship between soil water content and water retention from Ruehr et al., (2014)
168 and the root profile prescribed in the SPA model (Table 1).

169

170 *2.2 SPA multi-layer canopy model description*

171

172 The Soil-Plant-Atmosphere model (SPA; Williams et al., 1996, 2001a) is a high vertical
173 resolution point model (up to 10 canopy layers and 20 soil layers) which simulates exchanges of
174 carbon, water, and energy between the land surface and atmosphere on sub-hourly timesteps. The
175 SPA model has been used for a variety of applications including site level analyses of carbon and
176 water fluxes (Williams et al., 1996, 2001a, 2001b; Ruehr et al., 2014); model intercomparisons
177 of stomatal and hydraulic functioning (Misson et al., 2004; Bonan et al., 2014); data assimilation
178 (Williams et al., 2005; Sus et al., 2014); and modeling land-atmosphere feedbacks (Hill et al.,
179 2008; Smallman et al., 2013). In this study, we implemented several model updates including

180 those from a recent study which used the SPA model to simulate the carbon cycle at US-Me2
181 under current and future climate conditions (Ruehr et al., 2014).

182
183 The SPA model includes a detailed radiative transfer scheme for long-wave, near infra-red, and
184 direct and diffuse photosynthetically active radiation to determine transmittance, reflectance, and
185 absorption in each canopy layer for sunlit and shaded leaf fractions. Leaf energy balance is
186 coupled to a widely used biochemical model of photosynthesis (Farquhar and von Caemmerer,
187 1982) and leaf transpiration through an optimization scheme for stomatal conductance. In this
188 study's implementation, rather than using the Penman-Monteith equation for leaf transpiration,
189 we calculated transpiration directly from Fick's law as:

$$190 \quad T = g_w * D_l \quad (1)$$

191 where T is the transpiration rate per unit leaf area ($\text{mmol m}^{-2} \text{s}^{-1}$), g_w is the two-sided leaf total
192 conductance (series of stomatal and leaf boundary layer) to water vapor ($\text{mmol m}^{-2} \text{s}^{-1}$), and D_l is
193 the leaf-specific vapor deficit (mol mol^{-1}).

194
195 The SPA model calculates stomatal conductance for each canopy layer based on a hypothesis
196 that stomatal conductance is regulated to prevent hydraulic failure (Williams et al., 1996, 2001a).
197 The transport of water through the soil-plant-atmosphere continuum flows down a potential
198 gradient at a rate proportional to the whole-plant conductance. The plant conductance is a static
199 function of hydraulic architecture, xylem construction, and leaf conductance and the soil-to-root
200 conductance is a function of soil hydraulic conductivity and root density. Following Ruehr et al.,
201 (2014), we reduced whole plant conductance in response to declining soil water potential
202 according to a sigmoid function and reduced the soil tortuosity and soil surface roughness length
203 to increase soil water evaporation and better match observations.

204
205 In this application, we used six canopy layers, each with equivalent LAI but varied thickness to
206 approximate canopy structure (Reinhardt et al., 2006). The vertical soil profile was defined by 20
207 soil layers of 0.1m thickness with soil texture defined as in Law et al., (2001). We modified the
208 SPA model to run using prescribed soil water content and implemented a site-specific empirical
209 relationship between soil water content and soil water potential following Ruehr et al., (2014).
210 Configuration of canopy structure, photosynthesis parameters, and rooting profile can be found

211 in Table 1, and we provide more information on model updates in the Supplementary
 212 Information.

213

Model	Description	Units	Value	Source
All	Leaf area index	$\text{m}^2 \text{m}^{-2}$	2.8	Irvine et al., 2004
All	Leaf carbon per leaf area	gC m^{-2} leaf area	122.4	Ruehr et al., 2014
All	Maximum rooting depth	m	1.1	Ruehr et al., 2014
All	Total root biomass	g m^{-2}	70	Ruehr et al., 2014
All	V _{cmax} at 25°C	$\mu\text{mol m}^{-2} \text{s}^{-1}$	31.4	Ruehr et al., 2014
All	J _{max} at 25°C	$\mu\text{mol m}^{-2} \text{s}^{-1}$	52.4	Ruehr et al., 2014
All	Canopy height	m	18	Ruehr et al., 2014
SPA	Height of canopy layers	m	18,15.9,15.1,14.2,13.3,11.8,9	defined to have equal LAI and follow canopy structure.
SPA	Average foliar nitrogen	gN m^{-2} leaf area	2.1	Schwarz et al., 2004
SPA	Plant capacitance	$\text{mmolH}_2\text{O m}^{-2}$ leaf area MPa^{-1}	2500	Bonan et al., 2014
SPA	Root resistivity	MPa s g mmol^{-1}	20	Ruehr et al., 2014
Gain-Risk	Leaf area:basal area	$\text{m}^2 \text{m}^{-2}$	878	Irvine et al., 2004
Gain-Risk	Basal area:ground area	$\text{m}^2 \text{Ha}^{-1}$	31.9	Irvine et al., 2004
Gain-Risk	Rhizosphere resistivity	(%)	50	Venturas et al., 2018

214 **Table 1.** Canopy structure, root distribution and photosynthesis parameter values used in models.

215

216 2.3 Stomatal sub-models in SPA

217

218 We compared four sub-models with unique assumptions regarding stomatal behavior within the
 219 SPA model framework, each including explicit hydraulic mechanisms that down regulate
 220 stomatal conductance in response to more negative plant water potential. We implemented
 221 hydraulic constraints to the Ball et al., (1987) model (hereafter referred to as BB-H) and the
 222 Medlyn et al., (2011) model (MED-H); and use two different definitions of stomatal efficiency in

223 the SPA optimization scheme based on intrinsic water use efficiency (WUE_i) and the ratio of
 224 CO₂ assimilation to transpiration (WUE).

225

226 The predominant semi-empirical model for stomatal functioning was developed by Ball et al.,
 227 (1987) who defined a simple linear approximation of the relationship between photosynthesis
 228 and stomatal conductance to water (g_w ; mol H₂O m⁻² s⁻¹) based on gas exchange data:

$$229 \quad g_w = g_0 + g_{1B} \left(\frac{A*rh}{C_a} \right) \quad (2)$$

230 where A is the net assimilation rate ($\mu\text{mol CO}_2 \text{ m}^{-2} \text{ s}^{-1}$), rh is the relative humidity at the leaf
 231 surface (mol mol⁻¹), C_a is the atmospheric CO₂ concentration at the leaf surface ($\mu\text{mol mol}^{-1}$) and
 232 g_0 and g_{1B} are fitted parameters. While g_0 and g_{1B} are determined by fitting the equation to leaf-
 233 gas exchange data, both represent physiologically meaningful quantities (Franks et al., 2017).

234 The intercept parameter, g_0 , is the minimum stomatal conductance and is usually close to zero.

235 We set g_0 to 0.1 as in Franks et al., (2017) throughout this study. The slope parameter, g_{1B} , is
 236 generally representative of g_w/A , the reciprocal of the intrinsic water use efficiency, A/g_w
 237 (Farquhar, 1989; Feng et al., 1999). The Ball et al., (1987) model assumes that stomata respond
 238 to relative humidity at the leaf level, but it is more likely that stomata sense water fluxes (Aphalo
 239 & Jarvis, 1991) and respond to changes in water status of the leaf tissue (Buckley, 2005; 2019).

240

241 An alternative framework for stomatal function was developed by Cowan and Farquhar (1977)
 242 based on the premise that optimal stomatal behavior maximizes carbon gain minus the carbon
 243 cost of water loss, $A - \lambda E$, where λ is often defined as the water use efficiency. By combining
 244 theory of optimal stomatal control (Cowan & Farquhar, 1977) and photosynthesis (Farquhar et
 245 al., 1980), Medlyn et al., (2011) derived the following expression for stomatal conductance:

$$246 \quad g_w = g_0 + 1.6 \left(1 + \frac{g_{1M}}{\sqrt{VPD}} \right) \frac{A}{C_a} \quad (3)$$

247 Where VPD is the vapor pressure deficit (kPa), and g_0 and g_{1M} are fit parameters. Despite having
 248 a similar form to the Ball et al., (1987) model, the fit parameter g_{1M} in the Medlyn et al., (2011)
 249 model has a different theoretical interpretation: g_{1M} is proportional to the marginal water cost of
 250 carbon (λ) and the CO₂ compensation point (Γ):

$$251 \quad g_{1M} = \sqrt{\frac{3\Gamma\lambda}{1.6}} \quad (4)$$

252 In this application, we introduce a hydraulic constraint into the Ball et al., (1987) and Medlyn et
 253 al., (2011) stomatal models similarly to the approach of Wolf et al., (2016). At short time scales,
 254 λ is usually treated as an unknown fitted constant but λ can also be determined from system
 255 boundary conditions and generally follows an exponential function with soil moisture (Cowan
 256 1986, Mäkelä et al., 1986; Manzoni et al., 2013), therefore supporting our semi-empirical model
 257 variations. Specifically, the instantaneous leaf water potential in each canopy layer modifies the
 258 g_l parameter according to a Weibull function based on the leaf hydraulic vulnerability curve as:

$$259 \quad g_l = g_{l_0} * e^{-\left(\frac{-LWP}{b}\right)^c} \quad (5)$$

260 Where g_{l_0} is the value of g_l when soil water potential is near zero, LWP represents the
 261 instantaneous leaf water potential (MPa), and the Weibull b and c parameters are fitted according
 262 to measurements of ponderosa pine hydraulic leaf hydraulic vulnerability (Figure S1). Hereafter
 263 we refer to the Ball et al., (1987) and Medlyn et al., (2011) models with hydraulic constraints as
 264 BB-H and MED-H, respectively.

265
 266 In the default SPA model, stomatal conductance shares some commonalities with theory of
 267 optimal stomatal behavior (Cowan & Farquhar, 1977). Stomatal conductance is calculated to
 268 maximize assimilation, given transport of water from soil-to-leaf, plant water storage, and
 269 hydraulic safety margins (Figure 1). The optimization scheme incrementally increases stomatal
 270 aperture until further opening either: 1) does not increase carbon gain per unit water loss (defined
 271 by the stomatal efficiency parameter); or 2) causes leaf water potential to drop below a pre-set
 272 minimum value ($minLWP$). The stomatal efficiency is defined as the assimilation divided by the
 273 stomatal conductance to water (A/g_w) and we refer to this version of the SPA model as WUEi.
 274 Bonan et al., (2014) introduced an alternate definition of stomatal efficiency into the SPA model,
 275 A/T , which we refer to as WUE. Both implementations can represent conservative to more
 276 intensive plant water use behavior. For example, conservative behavior is achieved by setting a
 277 higher stomatal efficiency value and increasing the amount of appreciable carbon gain per unit
 278 increase in stomatal opening. As a result, excessive transpiration is avoided in the morning when
 279 atmospheric demand is low in order to preserve water to buffer the effects of high mid-day
 280 atmospheric demands (i.e., more isohydric behavior). Low values of stomatal efficiency result in
 281 intensive water use (higher optimal g_w and more transpiration).

282

283 2.4 Gain-Risk big-leaf model description

284

285 We also applied the model of Sperry et al., (2017), a big-leaf model with five soil layers
 286 (hereafter referred to as the Gain-Risk model). Stomatal functioning in the Gain-Risk model is
 287 based on optimization theory and assumes plants maximize carbon gain while minimizing
 288 hydraulic risk (Sperry & Love, 2015; Sperry et al., 2016, 2017; Wolf et al., 2016; Anderegg et
 289 al., 2018). The resulting coordination between stomatal and xylem functioning agrees well with
 290 observations (Meinzer et al., 2009) and more strongly agrees with leaf-level gas exchange data
 291 than the classic Cowan-Farquhar based optimization models (Anderegg et al. 2018; Wang et al.
 292 2020). Carbon gain is calculated as in the SPA model (Farquhar et al., 1980) and the carbon gain
 293 function, α , is defined at a given value of T as:

$$294 \quad \alpha = \frac{A_{net}}{A_{max}} \quad (6)$$

295 Hydraulic risk is defined as the fractional loss of hydraulic conductance. Vulnerability to
 296 cavitation curves (VC's) for each xylem element (roots, stem, and leaves) are represented by
 297 two-parameter Weibull functions:

$$298 \quad K = K_{max} * e^{-\left(\frac{-p}{b}\right)^c} \quad (7)$$

299 Where K is the hydraulic conductance, K_{max} is the maximum hydraulic conductance, p is the
 300 pressure imposed on each xylem element, and b and c are fit parameters (Figure S1). At each
 301 increment in T, the pressure drop across xylem elements ($p_{up} - p_{down}$) is calculated and the supply
 302 function is then defined as the relationship between T and canopy water potential (P):

$$303 \quad T = \int_{P_{up}}^{P_{down}} K(P) dp \quad (8)$$

304 The derivative of the supply function ($K_c = dT/dP$) represents the hydraulic conductivity loss
 305 which is at a maximum (K_{cmax}) when $T=0$, and the hydraulic risk function (θ) is defined as the
 306 fractional loss in K_c at a given value of T:

$$307 \quad \theta = 1 - \frac{K_c}{K_{cmax}} \quad (9)$$

308 The Gain-Risk model finds the optimal stomatal conductance by incrementing T from zero and
 309 calculating the marginal carbon gain, α , given the environmental conditions at that time step.
 310 The hydraulic risk is calculated from the change in P and the optimal T rate is that which
 311 maximizes the difference between the carbon gain function and the hydraulic risk function. The
 312

313 stomatal conductance is then calculated from the optimal T and the VPD at that time step as in
314 the SPA model. Fluxes are then scaled from leaf area to basal area to ground area using
315 measurements from Irvine et al., (2004) (Table 1). We ran the Gain-Risk model without xylem
316 refilling to capture permanent losses in hydraulic conductivity that lead to reductions in
317 transpiration and assimilation after a drought. To ensure that soil water stress was identical
318 across models we prescribed soil water potential in the Gain-Risk model from measurements of
319 soil water content and measured soil water retention curves as with the SPA model.

320

321 *2.5 Parameterization of stomatal sub-models and hydraulic function*

322

323 We prescribed model parameter values based on plant trait measurements available in the
324 literature rather than best-fit calibrations in order to reflect how formulations may be used in
325 Earth System Models. Additionally, our goal was to ensure that all parameters with the same
326 mechanistic meaning were equivalent. Therefore, differences in model performances better
327 reflect adequacy of model structures versus differences due to varying parameter calibrations.

328

329 Franks et al., (2017) demonstrated that equivalent g_l parameter values for the Ball et al., (1987)
330 and Medlyn et al., (2011) models can be derived as:

$$331 \quad g_{1B} \approx \frac{1.6}{rh} * \left(1 + \frac{g_{1M}}{\sqrt{vpd}} \right) \quad (10)$$

332 Additionally, the WUE stomatal efficiency parameter (ι) in the SPA model is equivalent to $1/\lambda$
333 thus equations 3 and 4 can be used to determine the equivalent value of ι for a given value of the
334 g_{1M} parameter. In this application we set the Medlyn et al., (2011) g_{1M} parameter to 2.35,
335 determined from gas-exchange data in Lin et al., (2015) representing needleleaf plant functional
336 types. We determined g_{1B} and ι from equations 10 and 4, respectively, with air temperature =
337 25°C , $rh = 0.45$, and $\Gamma = 40 \mu\text{mol/mol}$ (Table 2). The Gain-Risk model does not have an
338 equivalent parameter since the water use efficiency is diagnosed from the relationship between
339 carbon gain and hydraulic risk.

340

341 The Gain-Risk, WUEi and WUE models all use the leaf specific conductance, which was set to
342 $8.2 \text{ mmol m}^{-2} \text{ s}^{-1} \text{ MPa}^{-1}$ for a Ponderosa pine as per Johnson et al., (2009). The leaf and root

343 hydraulic vulnerability curves used in the Gain-Risk model were from previous studies of
 344 ponderosa pine (Sperry et al., 2019), while the stem VC was measured at the site but agrees well
 345 with literature values used by Sperry et al., (2019). Although the BB-H and MED-H approaches
 346 impose hydraulic limitation on stomatal functioning differently than the Gain-Risk model, we
 347 used consistent Weibull *b* and *c* parameters from the leaf VC in equation 6 (Figure S1).

348

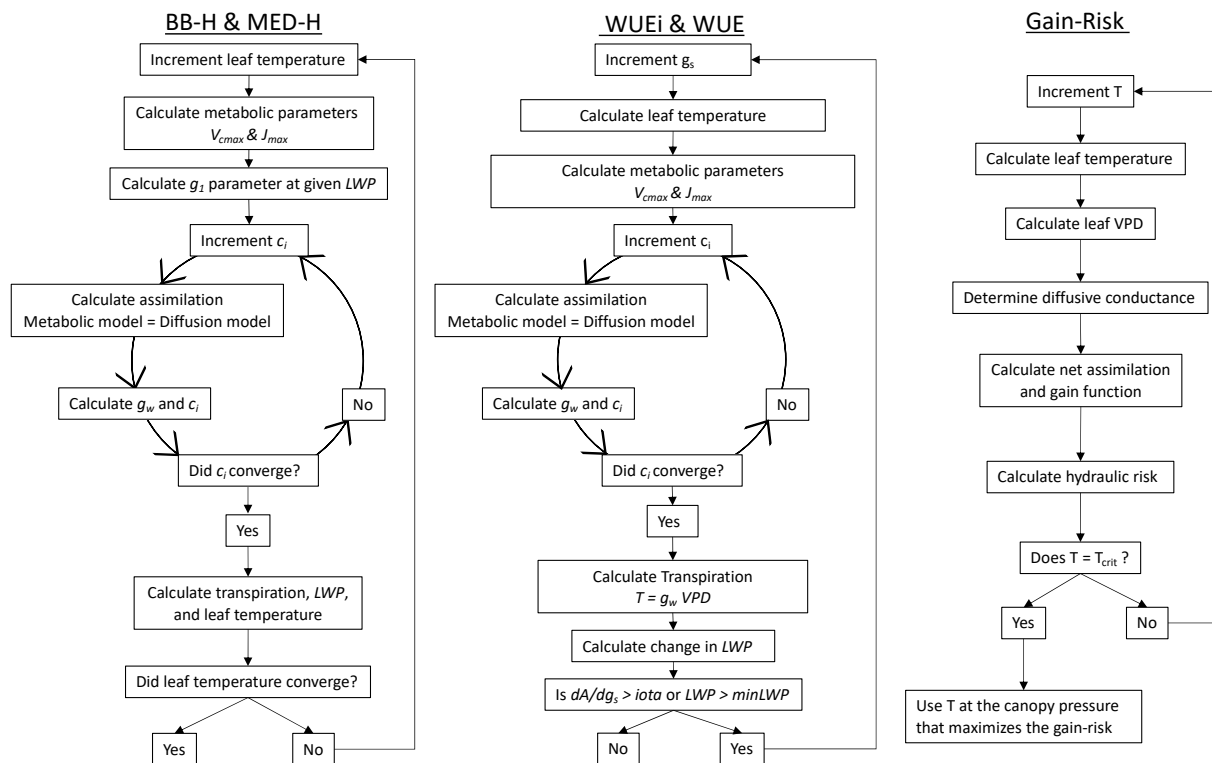
BB-H	Parameter	Unit	Value	Range
<i>g_{1B}</i>	Fit parameter	unitless	14.2	(6, 14)
<i>Weibull b</i>	VC parameter	-MPa	2.8	(1, 5)
<i>Weibull c</i>	VC parameter	unitless	3.7	(1, 5)
MED-H				
<i>g_{1M}</i>	Fit parameter	kPa ^{0.5}	2.35	(1, 5)
<i>Weibull b</i>	VC parameter	-MPa	2.8	(1, 5)
<i>Weibull c</i>	VC parameter	unitless	3.7	(1, 5)
WUEi/WUE				
<i>g_{plant}</i>	Leaf specific conductance	Mmol m ⁻² s ⁻¹ MPa ⁻¹	8.2	(3, 30)
<i>minLWP</i>	Minimum leaf water potential	MPa	-2	(-5, -1.7)
<i>ι</i>	stomatal efficiency (WUEi: dA/dg _s , WUE: dA/dE)	(umol CO ₂ /molH ₂ O)	0.0135 / 1350	(0.00375,0.03) (375, 3000)
Gain-Risk				
<i>K_{max}</i>	Maximum conductivity	Kg h ⁻¹ MPa ⁻¹ m ⁻²	120	(43, 424)
<i>LSC</i>	Leaf specific conductance	Mmol m ⁻² s ⁻¹ MPa ⁻¹	8.2	(3, 30)
<i>Weibull b</i>	VC parameter	-MPa (root/stem/leaf)	1.56 / 4 / 2.8	(0.8, 2.2)
<i>Weibull c</i>	VC parameter	unitless (root/stem/leaf)	1.4 / 3.4 / 3.7	(2, 3.5)

349 **Table 2.** Stomatal conductance model parameter definitions, values, and perturbation ranges for
 350 sensitivity analysis.

351

352 In this study we always assumed plants modify stomatal function instantaneously. The original
 353 formulations of WUEi, WUE, and Gain-Risk models modify the water use efficiency in response

354 to hydraulic constraints on instantaneous timescales. For consistency, we made the same
 355 assumption in the BB-H and MED-H models by modifying the g_l parameter based on
 356 instantaneous LWP. Though there is insufficient observational evidence to indicate whether
 357 stomata respond instantaneously to stimuli, we tested our assumption by comparing simulated
 358 canopy conductance using the predawn versus instantaneous LWP to represent slower versus
 359 faster responses of water use efficiency to hydraulic stress. We found that the simulated canopy
 360 conductance better matched the diurnal shape of the observed canopy conductance when the
 361 instantaneous LWP was used (Figure S2). Continuous measurements of canopy water potential
 362 are needed to help constrain these processes and inform model representation. Additionally, all
 363 models used in this study assumed hydraulic stress only modified stomatal function, but there is
 364 ongoing debate on how non-stomatal responses to hydraulic stress should be implemented in
 365 ecosystem models (Zhou et al., 2013).
 366



367
 368 **Figure 1.** Schematic of leaf flux calculations using the BB-H and MED-H models in the SPA
 369 model (left), the WUEi and WUE optimizations in the SPA model (center), and the Gain-Risk
 370 model (right).
 371

372 To elucidate model parameter sensitivity and parameterization uncertainty across models we
373 performed a perturbed parameter experiment. Parameters related to hydraulic and stomatal
374 functioning were modified simultaneously within ranges defined by literature or expert
375 solicitation (Table 2). We performed a Fourier amplitude sensitivity test (FAST; Saltelli and
376 Bolado, 1998) to quantify the contribution of each parameter to the total variance in T. See
377 supplementary information for further description (Text S2, Figures S3, S4).

378

379 *2.6 Functional performance evaluation*

380

381 We performed a series of diagnostics to quantify and compare model functional performance
382 under conditions spanning well-watered to atmospheric and/or soil drought stressed. We
383 employed three evaluation strategies, including the analysis of (i) diurnal processes individually;
384 (ii) effective functional relations between processes and an environmental driver; (iii) joint
385 causal relations and functional performance metrics based on information theory. We grouped
386 the data (June–August of 2006–2018) according to inter-quartile ranges of SWP and VPD to
387 examine varying degrees to atmospheric and/or soil water stress. We aggregated SPA leaf-level
388 process simulations over all canopy layers, scaled by the assimilation in the sunlit and shaded
389 fraction of each layer to compare to the ecosystem-scale observations and to maintain
390 consistency with the Gain-Risk model that takes a big-leaf approach (with sunlit and shaded
391 fractions).

392

393 We first explored modeled ecosystem-scale processes on diurnal time scales to understand how
394 model assumptions manifest. We compared models in terms of diurnal simulations of
395 transpiration (T); canopy conductance (G_c); canopy water potential (P); gross primary production
396 (GPP); the ratio of internal to external partial pressure of CO_2 (C_i/C_a); and the difference between
397 canopy and air temperature ($T_{\text{can}} - T_{\text{air}}$). We then compared the simulated diurnal cycle of T under
398 four different levels of atmospheric and/or soil water drought stress to examine how model
399 assumptions affect the diurnal cycle of T in response to environmental stress. We also focused on
400 differences between observed and modeled canopy temperature (T_{can}) because it plays a critical
401 role in the calculation of photosynthetic rates and in the optimization of stomatal conductance.
402 T_{can} can diverge from the air temperature by several degrees, particularly when air temperatures

403 are high (Kim et al., 2016) which can have large consequences for leaf metabolic processes (Still
404 et al., 2019). To illustrate the consequences of T_{can} biases we performed simulations with the
405 MED-H model where we prescribed model leaf temperature as the measured canopy
406 temperature.

407
408 We then evaluated how different model representations influence the sensitivity of G_c to VPD
409 under both low and high soil water stress following Novick et al., (2016). We derived G_c
410 empirically from sapflow and meteorological data and scaled the empirical and modeled G_c
411 estimates by their respective seasonal maximum. We fit an exponential decay function to the
412 rescaled data and compared G_c sensitivity to VPD in observations and models during low water
413 stress days (SWP > 75th percentile) high water stress days (SWP < 25th percentile) separately.
414 We quantified uncertainty in the empirical pattern by modifying the sapflow-derived
415 transpiration by $\pm 40\%$ and re-calculating G_c .

416
417 We also examined differences in model relations between water use efficiency and water
418 potential via C_i/C_a . The ratio C_i/C_a is thought to be a balance point between the stomatal supply
419 and photosynthetic demand for CO_2 and therefore is a measure of water-use efficiency and its
420 response to environmental conditions. C_i/C_a can be inferred from observed ratios of ^{13}C to ^{12}C in
421 cellulose in leaf tissue or tree rings ($\Delta^{13}\text{C}$), which have been previously used to constrain model
422 uncertainties (Lavergne et al., 2019). We compared estimated $\Delta^{13}\text{C}$ from model simulations
423 using the equation from Farquhar et al., (1982):

$$424 \quad \Delta^{13}\text{C} \approx a + (b - a) \frac{C_i}{C_a} \quad (11)$$

425 where a and b represent the isotopic fractionations due to diffusion of CO_2 in air (4.4‰) and
426 Rubisco carboxylation (27‰), respectively. Here we exclude the explicit fractionation term for
427 photorespiration and assume infinite boundary layer and mesophyll conductances and negligible
428 fractionation during mitochondrial respiration (Evans and von Caemmerer, 2013).

429
430 We used functional performance metrics based on information theory to quantify the ability of
431 models to reproduce the causal influence of atmospheric water demand and soil water supply
432 together on T as a mapping of inputs to outputs. We therefore evaluated how models represent
433 hydraulic function and feedbacks on gas exchange overall with non-parametric metrics, which

434 are especially relevant because ecosystem-scale data and processes are highly uncertain
435 (Bassiouni and Vico, 2021). Information theory is based on Shannon Entropy (Shannon, 1948), a
436 measure of uncertainty in a random variable or the information required to fully predict that
437 variable. Additionally, mutual information is a measure of the reduction of uncertainty or shared
438 information that knowledge of another variable can provide (Cover & Thomas 2012).
439 Quantifying this shared information among environmental variables, or information flows, has
440 been proven useful in inferring causal interactions among variables in complex ecohydrological
441 systems (Ruddell & Kumar, 2009; Goodwell et al., 2020).

442
443 Specifically, we quantified the information VPD and SWP together provide about observed T.
444 This quantity, the multi-variate mutual information, can be partitioned into four non-negative
445 components (Goodwell and Kumar, 2017) to measure patterns in plant hydraulic controls: unique
446 information (U_{VPD} and U_{SWP}) that only VPD or SWP provide about T; synergistic information
447 (S) that is provided only when both variables are known together; and redundant information (R)
448 that either variable can provide. We therefore evaluated the influence of both VPD and SWP on
449 T which is otherwise challenging to disentangle with established parametric approaches (e.g.,
450 Novick et al., 2016).

451
452 Each model structure may produce the four types (U_{VPD} , U_{SWP} , S , and R) of information
453 differently, and here we quantified model functional performance by comparing information
454 flows in the models to those in the observations at the daily time scale following Bassiouni &
455 Vico, (2021). As such, we calculated six functional performance metrics as the relative
456 difference between observed and modeled total mutual information ($A_{f,T}$); individual
457 information partitioning components ($A_{f,VPD}$, $A_{f,SWP}$, $A_{f,S}$, $A_{f,R}$); and the sum of the absolute
458 values of the partitioning accuracies ($A_{f,p} = |A_{f,SWP}| + |A_{f,VPD}| + |A_{f,S}| + |A_{f,R}|$). Additionally,
459 we quantified predictive performance (A_p) in terms of the relative fraction of missing
460 information about T in the model compared to observations. This metric is calculated as the
461 relative difference between the entropy of observed T and the mutual information between
462 observed and modeled T. We estimated uncertainty by re-calculating the functional performance
463 metrics from 10,000 bootstrapped samples of 80% of the data. For all performance metrics a
464 value of 0 is a perfect match between models and observations.

465

466 **3 Results**

467

468 *3.1 Diurnal cycle of ecosystem processes*

469

470 We examined simulated processes on hourly timescales to elucidate how model assumptions
471 manifest in ecological functioning. For illustration, we show simulated days in mid-August 2010
472 when root-weighted soil water potential was below -1 MPa and daily maximum VPD increased
473 from 1 to nearly 3 kPa (Figure 2). Generally, observed T peaked in the morning and tapered off
474 throughout the day. All models adequately represented the diurnal transpiration except the Gain-
475 Risk model which predicted T peaking in the afternoon. Similarly, observed G_c peaked in the
476 morning and was reduced quickly throughout the day. All models simulated the shape of the
477 diurnal cycle in G_c well, however the magnitude of G_c in the BB-H, MED-H, WUEi, and WUE
478 models was lower than the observed estimate. The Gain-Risk model simulates a slight increase
479 in G_c in the afternoon due to the way G_c is calculated: the model determines the optimal
480 transpiration rate from the Gain-Risk functions, and then stomatal conductance to water vapor,
481 g_w , is calculated as $T=g_w*VPD$. Thus, as transpiration and VPD increase through the day g_w must
482 decline, and as transpiration declines through the afternoon, g_w increases again.

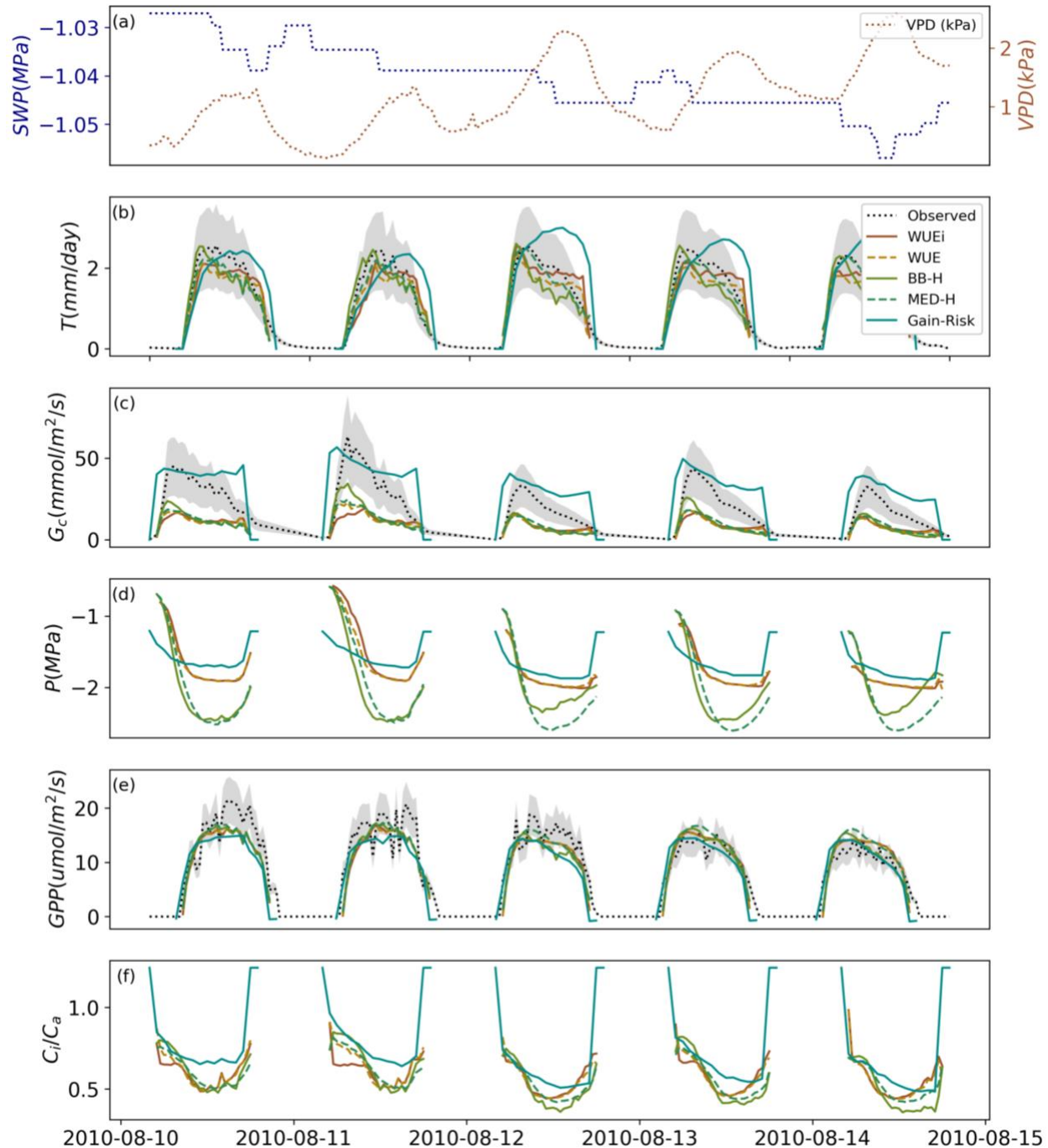
483

484 The simulated canopy water potential, P, illustrates the impact of the minimum LWP threshold
485 set in the WUEi and WUE models. Once the threshold is reached the g_w is reduced to avoid
486 cavitation and the minimum LWP is maintained throughout the day. Despite using more
487 sophisticated hydraulic constraint functions, the Gain-Risk model simulates a similar diurnal
488 shape in P. The hydraulic limitation in the BB-H and MED-H models modifies the g_l parameter
489 as a function of instantaneous LWP; this implementation reduces GPP and T but there are no
490 direct constraints on how low the canopy water potential can get and consequentially the mid-
491 day canopy water potential reaches much lower values compared to the other models.

492

493 The magnitude and shape of gross primary productivity (GPP) is well captured by all models;
494 however, the sub-daily variability is not well simulated. All models simulate a much smoother
495 and consistent diurnal cycle of GPP whereas the observations are much more variable. The

496 simulated ratio of intercellular CO₂ concentration to atmospheric CO₂ concentration (C_i/C_a) often
 497 reached minimum values around 0.5 by mid-afternoon.
 498

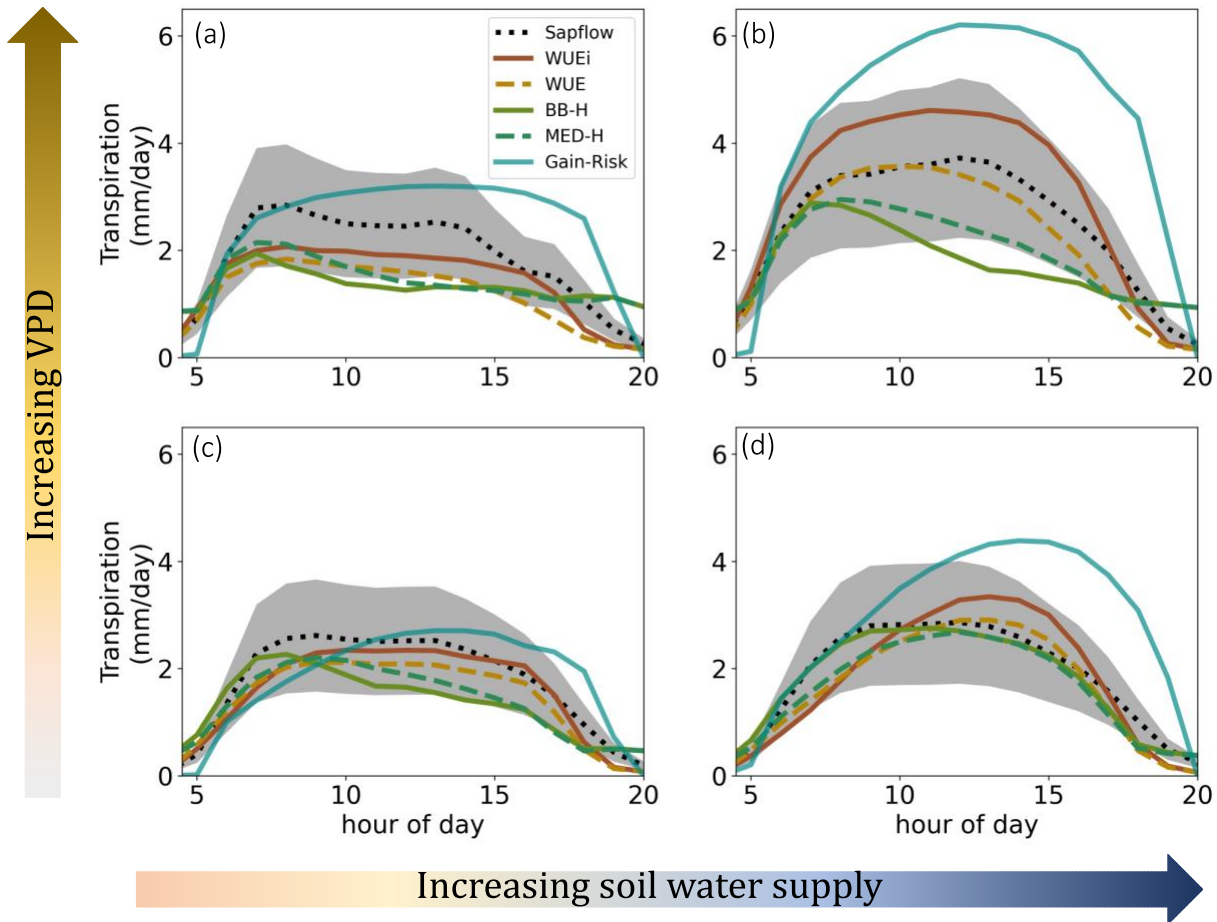


499
 500 **Figure 2.** Diurnal cycle of measured or model simulated leaf level processes in mid-August
 501 2010. (a) measured above-canopy VPD (kPa) and root-weighted soil water potential (MPa), (b)
 502 transpiration (mm/day) with observations derived from sapflow measurements (black dotted

503 lines), shading represents uncertainty of $\pm 40\%$ as per Ruehr et al., (2014), (c) canopy
504 conductance ($\text{mmol/m}^2/\text{s}$); observations estimated from sapflow measurements (black dotted
505 lines) with shading representing uncertainty in sapflow estimates of transpiration, (d) simulated
506 canopy water potential (MPa); (e) gross primary productivity ($\text{umol m}^{-2} \text{s}^{-1}$); and (f) simulated
507 ratio of internal leaf CO_2 to atmospheric CO_2 concentrations.

508

509 All models adequately simulated the annual cycle of T and GPP for 2006-2018 (Figure S5) but to
510 better understand model functional performance we evaluated model responses in varying
511 environmental conditions. We assessed how models modify the shape of the diurnal cycle in T in
512 response to VPD and SWP stress, according to four categories: high VPD and low SWP, high
513 VPD and high SWP, low VPD and low SWP, and low VPD and high SWP (Figure 3). Low SWP
514 is more negative and thus indicates higher drought stress. Generally, observed T peaks around
515 9am and stays relatively constant throughout the day, illustrating the conservative water use
516 strategies typical of ponderosa pines. On days with high VPD there is a midday depression in T,
517 but if soil moisture is not limiting transpiration resumes in the afternoon. All models alter the
518 magnitude and shape of the simulated diurnal cycle in response to VPD and soil water potential,
519 albeit to differing degrees. When soil water stress is high (Figure 3a,c) all models limit mid-day
520 T and shift to more conservative water use. Models show this largest divergence from one
521 another when VPD is high and soil water supply is also high (Figure 3b); high atmospheric
522 demand increases the simulated T (relative to panel d) by varying amounts. Notably, in all
523 categories the diurnal cycle simulated with the Gain-Risk model is markedly different from the
524 observations and the other models. The Gain-Risk model simulates too much T when soil water
525 supply is high (Figure 3b,d) and simulated T peaks in the late afternoon since the VPD constraint
526 on T is applied indirectly via the carbon gain function.



527
 528 **Figure 3.** Average diurnal cycle of observed transpiration (black dashed) and modeled
 529 transpiration (colors) for days in July (2006–2018) with (a) maximum daily VPD above 75th
 530 percentile and root-weighted SWP below 25th percentile (18 days), (b) VPD > 75th percentile and
 531 SWP > 50th percentile (41 days) (c) VPD < 50th percentile and SWP < 25th percentile (28 days)
 532 and (d) VPD < 50th percentile and SWP > 50th percentile (119 days). Uncertainties in sapflow
 533 derived estimates of transpiration are estimated to be 40% (grey shading) as per Ruehr et al.,
 534 (2014).

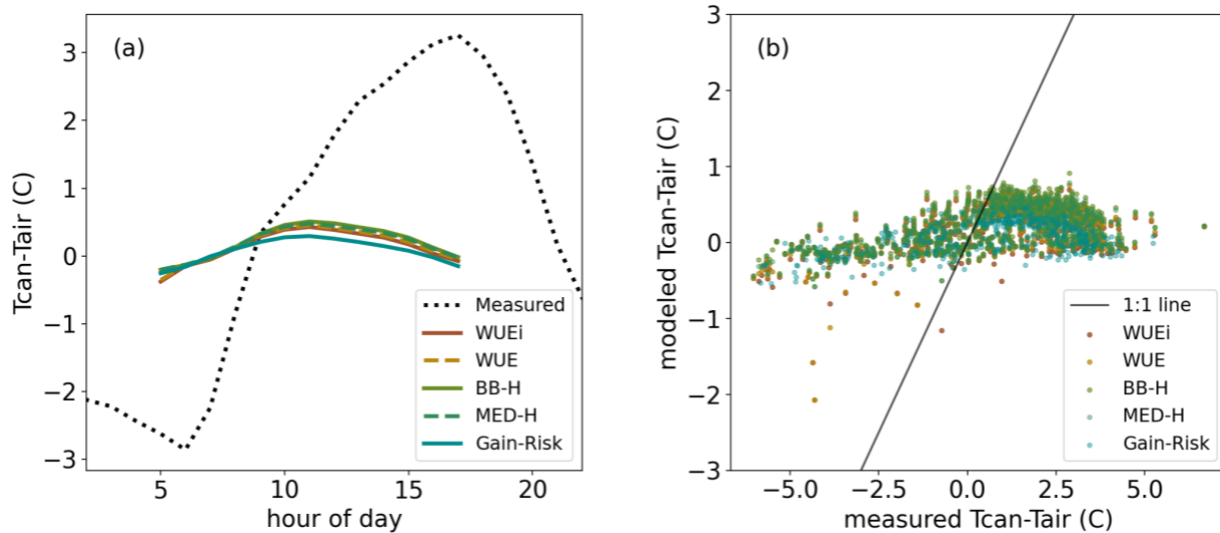
535

536 3.2 Canopy temperature performance

537

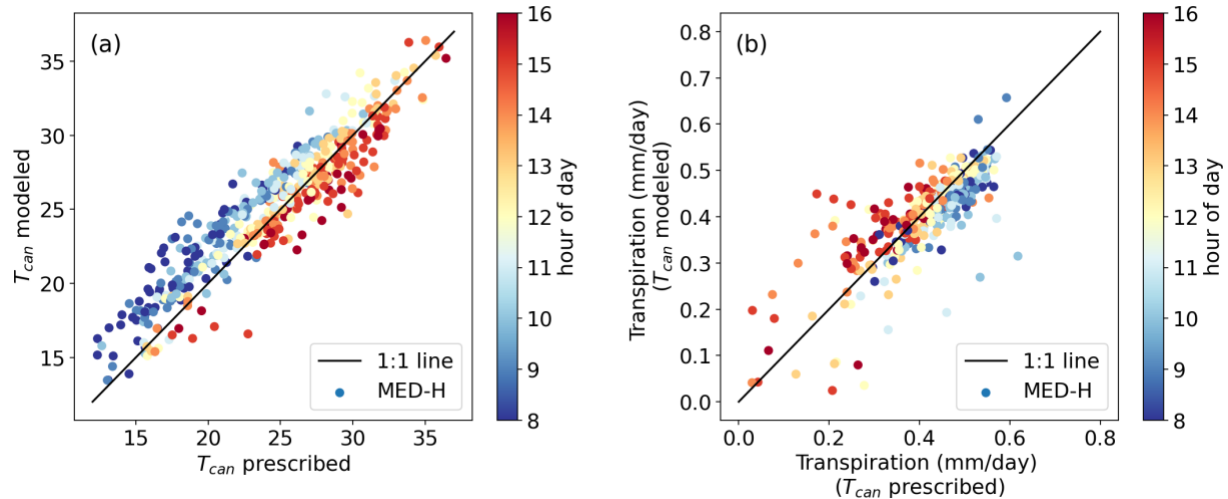
538 In August when air temperatures typically peak at this site the observed canopy temperature
 539 (T_{can}) diverges from the air temperature (T_{air}) by mid-morning and can be two or three degrees
 540 warmer than T_{air} by mid-afternoon (Figure 4a). All models simulate a very slight increase in T_{can}
 541 above T_{air} (<1°C) but fail to capture the large observed divergence of T_{can} from T_{air} . The damped

542 response in modeled leaf temperature persists across models despite different representation of
 543 leaf temperature feedback mechanisms. Furthermore, the bias is similar between the multilayer
 544 canopy models (SPA) and the big-leaf model (Gain-Risk), which indicates the bias is not
 545 ameliorated with increased vertical resolution.



546
 547 **Figure 4.** Measured and modeled canopy-air temperature in August 2015. Average diurnal cycle
 548 (a) and measured versus modeled daytime mean canopy-air temperature (b).

549
 550 Prescribing observed leaf temperature in the MED-H model results in cooler morning leaf
 551 temperatures and warmer afternoon leaf temperatures (Figure 5a). The cooler morning leaf
 552 temperatures lead to more morning transpiration (Figure 5b). In August of 2015, the cumulative
 553 morning (8am-12pm) transpiration was 9% higher when using the prescribed canopy
 554 temperature. In the afternoons, the prescribed the canopy temperature was warmer than the
 555 modeled canopy temperature, which resulted in lower transpiration rates. The cumulative
 556 afternoon (12pm-4pm) transpiration in August 2015 was 4% lower when using the prescribed
 557 canopy temperature. These results indicate that resolving biases in modeled canopy temperature
 558 would lead to increased morning transpiration and decreased afternoon transpiration. These
 559 changes counteract one another, and the net effect was a 5% increase in total growing season
 560 (JJA) transpiration (not shown).



561
 562 **Figure 5.** August 2015 canopy temperature (a) and transpiration (b) simulated with the MED-H
 563 model using the modeled canopy temperature (y-axis) or the prescribed canopy temperature (x-
 564 axis). Shading represents the hour of day; data is shown on 30min time intervals between 8am
 565 and 4pm.

566

567 3.3 Evaluation of the sensitivity of stomatal conductance to VPD

568

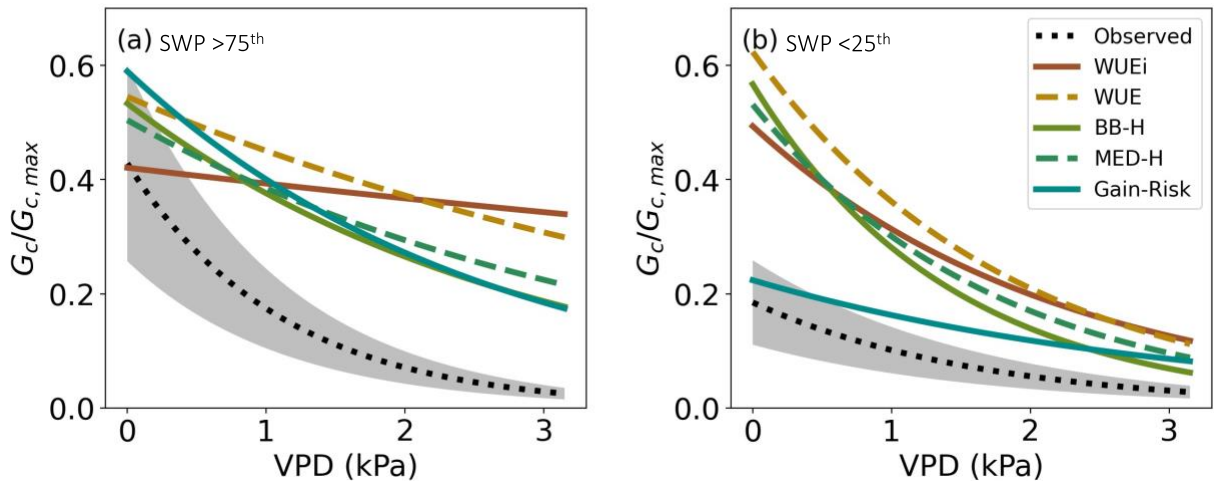
569 When water stress was low (SWP above the 75th percentile) the observed G_c had a strong
 570 sensitivity to increasing VPD (Figure 6a). None of the models captured the sensitivity to VPD
 571 well, all models were less sensitive to VPD than observations. While models were generally
 572 indistinguishable, the WUEi model had the lowest sensitivity to VPD. This was expected given
 573 that the WUEi model optimizes $\Delta A/\Delta g_s$ and thus does not have a direct dependency on VPD.
 574 The WUE optimization has a direct dependency on VPD since stomatal efficiency is defined as
 575 $\Delta A/\Delta T$ and thus G_c is more sensitive to VPD as was shown by Bonan et al., (2014). The BB-H
 576 and MED-H models have similar sensitivities to VPD even though the MED-H model directly
 577 relates g_w to VPD whereas in BB-H g_w is a function of rh . However, these results agree well with
 578 the findings of Franks et al., (2017) who illustrated that with equivalent parameterizations these
 579 two models have similar performance.

580

581 When water stress was high (SWP < 25th percentile) the observed G_c was reduced and the
 582 sensitivity to VPD was weaker since G_c was already depressed (Figure 6b). The Gain-Risk

583 model captured the magnitude of the depression in G_c when VPD was low, illustrating that soil
 584 water potential alone exhibits a strong constraint on G_c in this model. The other models did not
 585 depress G_c sufficiently in response to water stress but were more sensitive to VPD, decreasing G_c
 586 quickly in response to higher VPD.

587



588

589 **Figure 6.** Observed (black) and modeled (color) sensitivity of canopy conductance ($G_c/G_{c,max}$) to
 590 VPD when the soil water potential was greater than the 75th percentile (a), and when the soil
 591 water potential was less than the 25th percentile (b). Grey shading represents estimated error in
 592 G_c given 40% uncertainty in sapflow-derived transpiration.

593

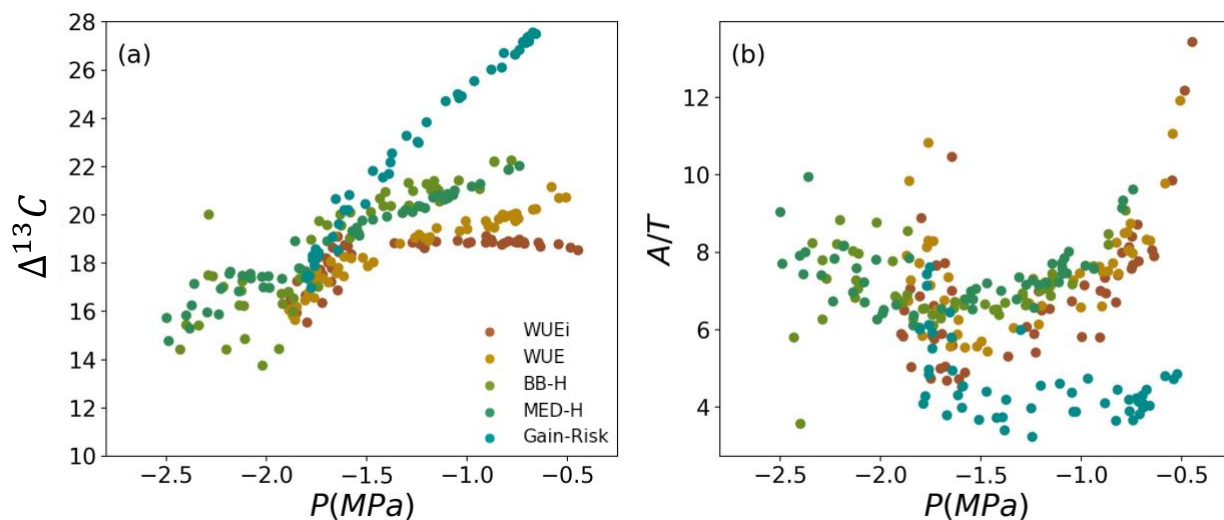
594 3.4 Variability in $\Delta^{13}C$ and water stress

595

596 We examined the simulated monthly mean daytime $\Delta^{13}C$ for June through August 2006–2018.
 597 While observational measurements of $\Delta^{13}C$ were not available at this site during the time period
 598 covered in this study, we found that the simulated values generally agreed with reported values
 599 from the literature. Bowling et al., (2002) reported carbon isotopic composition of ecosystem
 600 respiration from a nearby ponderosa site in 1996, 1997 and 2000. Assuming an atmospheric
 601 carbon isotope composition of -8‰ the reported values of $\Delta^{13}C$ from Bowling et al., (2002)
 602 ranged from 16 to 20‰. Furthermore, they found that $\Delta^{13}C$ decreased non-linearly with
 603 increasing VPD. Additionally, Ulrich et al., (2019) determined carbon isotope discrimination at
 604 this site using tree-ring cellulose. The reported annual values of $\Delta^{13}C$ for 1990-2002 ranged from
 605 17 to 19.5‰, again assuming an atmospheric carbon isotope composition of -8‰.

606

607 We examined simulated $\Delta^{13}\text{C}$ to differentiate among model responses to stress. We used the
 608 canopy water potential (P) as a measure of plant water stress and compared the simulated
 609 response in monthly mean daytime $\Delta^{13}\text{C}$ across models (Figure 7a). In the BB-H and MED-H
 610 models, $\Delta^{13}\text{C}$ decreased linearly with P . The Gain-Risk model also simulated a linear
 611 relationship, but $\Delta^{13}\text{C}$ declined more rapidly with P indicating that C_i was reduced more quickly
 612 under stress. The WUEi and WUE models do not allow P to drop below a threshold (-2 MPa in
 613 this study) but the $\Delta^{13}\text{C}$ can still be quite low when the minimum P is reached, resulting in an
 614 asymptotic relationship. $\Delta^{13}\text{C}$ is inversely related to the water-use efficiency, defined as A/T , and
 615 when P was low all models simulated an increase in water-use efficiency (Figure 7b). The Gain-
 616 Risk model had the lowest water-use efficiency under unstressed conditions, likely due to the
 617 lack of constraints on T when the hydraulic risk is low. This is consistent with the overestimation
 618 of T during unstressed conditions seen in previous results. Models clearly simulate distinct
 619 relationships between these measures of water-use efficiency and P during periods of both low
 620 and high environmental stress.



621

622 **Figure 7.** Simulated relationships between monthly mean daytime canopy water potential, P , and
 623 $\Delta^{13}\text{C}$ (a) or assimilation/transpiration (A/T) (b) simulated for June, July, and August 2006–2018.

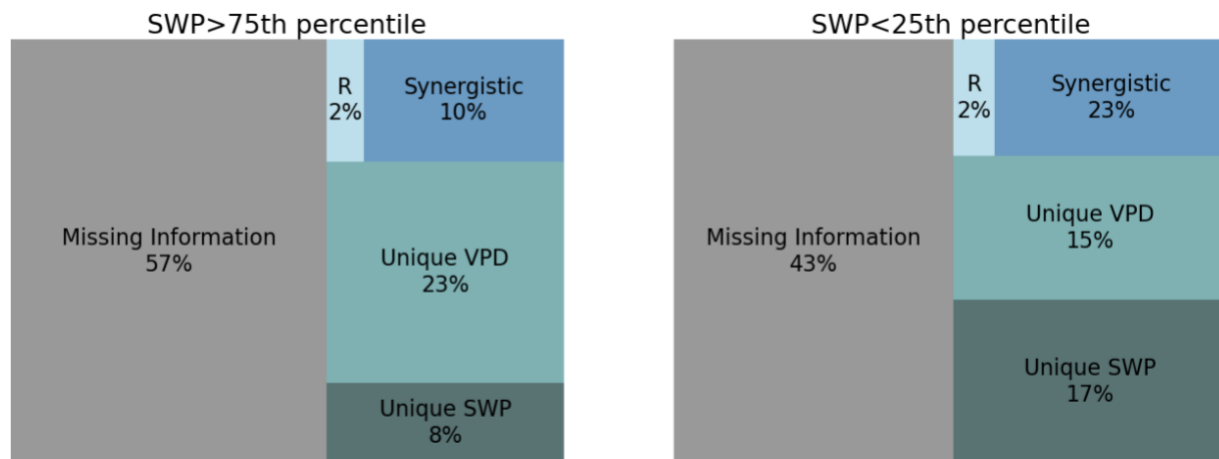
624

625 *3.5 Variability in information flows from VPD and SWP to T*

626

627 The influence of VPD and SWP together on T was measured by their multi-variate mutual
 628 information partitioned into redundant, synergistic, and unique information components. When
 629 water stress was low (SWP>75th percentile) the information from SWP and VPD together
 630 reduced 43% of uncertainty (entropy) in daily T (Figure 8). The remaining information about T
 631 can be attributed to the influence of the other environmental factors such as net radiation, which
 632 is a strong control on T in the spring when soil water is most available. The unique information
 633 from VPD reduced 23% of the uncertainty whereas the unique information from SWP and
 634 synergistic information reduced 8 and 10% of the uncertainty, respectively. This indicates that
 635 when water stress was low, VPD was a more influential control on T than SWP. When soil water
 636 stress was high (SWP<25th percentile) the observed SWP and VPD reduced 57% of uncertainty
 637 in T (Figure 8). In the water-stressed late summer months, photosynthetically active radiation
 638 and temperature are usually less limiting and thus VPD and SWP are more influential on T
 639 compared to the early spring months. The unique information from SWP and VPD reduced 17%
 640 and 15% of the uncertainty, respectively, and the synergistic information reduced an additional
 641 23%. In both the cases, the redundant information between VPD and SWP was small.

642



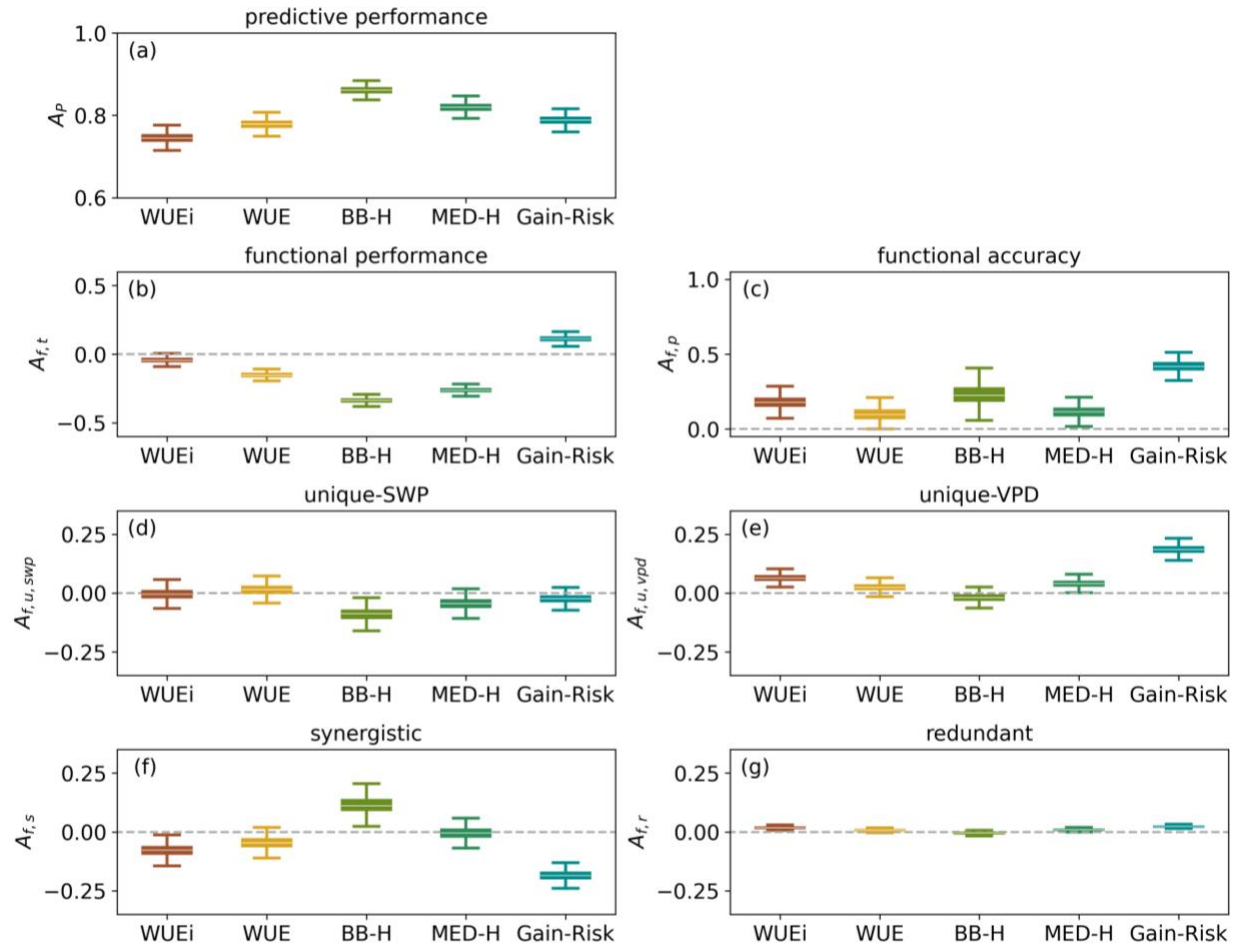
643

644 **Figure 8.** Reduction in uncertainty (mutual information) in daily transpiration rates attributable
 645 to vapor pressure deficit (VPD) and soil water potential (SWP), when SWP is above the 75th
 646 percentile (left) and below the 25th percentile (right). Mutual information is partitioned into
 647 synergistic, unique to VPD, unique to SWP, and redundant (R) information. The total area
 648 represents the entropy of transpiration and percentages are computed as the fraction of

649 transpiration entropy. Missing information represents the fraction of transpiration entropy that is
650 not shared with VPD and SWP.

651
652 We evaluated how well each model represented the functional relationships among daily VPD,
653 SWP and T by taking the difference between information flows calculated from measurements
654 and calculated from model simulations. When soil water stress was high (SWP < 25th percentile)
655 the more mechanistic models (WUE_i, WUE, Gain-Risk) had higher predictive performance
656 (lower A_p) than the semi-empirical models (BB-H, MED-H) and WUE_i had the most accurate T
657 estimates (Figure 9a). The WUE_i, WUE, and Gain-Risk models most accurately simulated the
658 total mutual information ($A_{f,t}$ closer to 0; Figure 9b) pointing to consistency in predictive and
659 functional performance. The BB-H and MED-H models most underestimated the total mutual
660 information contained in SWP and VPD about T and the Gain-Risk model was the only overly
661 deterministic model (positive $A_{f,t}$). In terms of the overall performance of information
662 partitioning WUE and MED-H were the most accurate ($A_{f,p}$ close to 0) (Figure 9c), despite not
663 having highest predictive performance. The Gain-Risk model had the poorest partitioning
664 accuracy (highest $A_{f,p}$), indicating that it may be reproducing the variability in T accurately but at
665 the expense of poorer representation of the individual information flows. All models (excluding
666 BB-H) accurately represented the unique information from SWP (Figure 9d) but the WUE_i and
667 Gain-Risk models overestimated the unique information from VPD (Figure 9e). The BB-H
668 model overrepresented the synergistic information whereas the Gain-Risk model underestimated
669 the synergistic information (Figure 9f). All models accurately captured the redundant
670 information (Figure 9g).

671



672
 673 **Figure 9.** Evaluation of model performance of daily transpiration (T) during growing season
 674 (May-August) of 2006 through 2018 when soil water potential (SWP) was below the 25th
 675 percentile (high soil water stress). (a) Predictive performance (A_p , bits bit⁻¹) quantifies the
 676 relative fraction of information missing in the model about T compared to observations. (b) Total
 677 functional performance ($A_{f,T}$, bits bit⁻¹) quantifies the relative difference between observed and
 678 modeled total multi-variate mutual information from SWP and VPD about T. (c) Functional
 679 accuracy ($A_{f,p} = |A_{f,swp}| + |A_{f,vpd}| + |A_{f,s}| + |A_{f,r}|$, bits bit⁻¹) quantifies the relative difference
 680 between observed and modeled mutual information partitioning from SWP and VPD about T.
 681 The components of functional accuracy are partitioned into (d) unique from soil water potential
 682 ($A_{f,swp}$, bits bit⁻¹), (e) unique from VPD ($A_{f,vpd}$, bits bit⁻¹), (f) synergistic ($A_{f,s}$, bits bit⁻¹), and
 683 (g) redundant ($A_{f,r}$, bits bit⁻¹) information. Boxes represent the interquartile range of
 684 bootstrapped samples; whiskers represent 5th and 95th percentiles; and white lines represent
 685 medians. For all metrics a value of zero indicates a perfect model-data match.

686
687 When water is not limiting (SWP>75th percentile) the predictive performance of all models was
688 indistinguishable (Figure S6). The BB-H had the best total functional performance; all other
689 models overestimated the strength of the total multi-variate mutual information from SWP and
690 VPD about T. The functional accuracy of the BB-H model outperformed all other models since
691 all other models overestimate the functional control of VPD on T and underestimate the
692 synergistic information.

693

694 **4 Discussion**

695

696 *4.1 Representing plant hydraulic strategies*

697

698 Plant water and carbon relations are strongly tied to the ways plants respond to hydrologic stress.
699 It's common to generalize plant hydraulic strategies along a continuum between isohydric and
700 anisohydric behavior. Although this framework is oversimplistic it can be useful (Kannenberget
701 al., 2021) when comparing behavior with common environmental forcings such as in this study.
702 The hydraulic limitation imposed in this study in the BB-H and MED-H models represents more
703 anisohydric behavior, as the model structure allows the canopy water potential to reach low mid-
704 day levels (Figure 2). At low canopy water potentials, the BB-H and MED-H models increase
705 the water-use efficiency (Figure 7) and constrain transpiration to peak in the morning (Figure 2
706 & 3). Given the functional form of the hydraulic limitation we impose, alternate
707 parameterizations cannot sufficiently represent the isohydric behavior characteristic of ponderosa
708 pines. A steeper hydraulic vulnerability constraint (achieved by modifying the b and c
709 parameters in eq. 6) would prevent the canopy water potential from reaching very low values but
710 only by modifying the g_l parameter and thus reducing assimilation to near zero.

711

712 The structure of the WUE_i and WUE models fundamentally represents isohydric water-use
713 strategies (Fisher et al., 2006). The minimum leaf water potential threshold limits stomatal
714 conductance at a prescribed canopy water potential which results in conservative water use. The
715 WUE_i and WUE models maintain relatively constant transpiration and canopy water potential
716 throughout the day (Figure 2). Less conservative water-use behavior can be achieved by setting

717 the minimum leaf water potential parameter to very low values (e.g., -6 MPa), then the stomatal
718 efficiency parameter constrains plant water-use. However, there is a trade-off; the low settings of
719 stomatal efficiency required to achieve anisohydric behavior also limit carbon assimilation.
720 Williams et al., (1996) applied the WUE_i model to a mixed deciduous broadleaf stand and was
721 able to capture anisohydric behavior early in the growing season when canopy water potentials
722 remained above the *minLWP* (set to -2.5MPa) but in the late growing season when canopy water
723 potentials were low the model constrained mid-day water-use and was unable to capture the
724 observed anisohydric behavior.

725

726 The Gain-Risk model constrains the canopy water potential to avoid hydraulic damage. With the
727 parameterization used in this application the model demonstrates conservative water use,
728 maintaining relatively constant mid-day canopy water potentials (Figure 2). The Gain-Risk
729 model can be parameterized to relax constraints on canopy water potential and can capture a
730 range of water-use strategies as demonstrated by Sabot et al., (2020). However, the
731 parameterization used here does not adequately capture the timing of water-use throughout the
732 day (Figure 3). Ponderosa pines maximize canopy conductance and use water early in the day
733 before the VPD gets too high (Figures 2 & 3), thus avoiding water loss while still maximizing
734 carbon gain. The Gain-Risk model captures the early morning peak in canopy conductance
735 (Figure 2), but it simulates transpiration peaking in the late afternoon, even under drought stress
736 when the hydraulic risk is high. It is possible that alternate plant trait combinations would alter
737 the diurnal cycle of transpiration. In addition, transpiration in the Gain-Risk model is very
738 sensitive to soil water potential (see Figure 6 in Venturas et al., 2018) and any error in the diurnal
739 cycle of soil or rhizosphere water potential propagates to transpiration. Future work is needed to
740 determine if the Gain-Risk model can capture conservative water-use strategies on sub-daily
741 temporal scales.

742

743 *4.2 Canopy temperature*

744

745 Accurately modeling canopy temperatures is critical for representing ecological processes,
746 particularly as heat waves become more frequent and severe under changing climate conditions.

747 While the biophysical drivers of canopy temperature vary among ecosystems, canopy

748 temperature is often more relevant to biological functioning than air temperature (Still et al.,
749 2019). The observed canopy temperature diverged from the air temperature by several degrees at
750 this site. At night, canopy temperatures cooled below air temperatures and during the day canopy
751 temperatures were nearly 3°C warmer than air temperatures (Figure 4). Similar behavior was
752 shown by Kim et al., (2016) who found canopy temperature to be a strong predictor of net
753 ecosystem exchange.

754
755 All models examined in this study were unable to capture the divergence of canopy temperature
756 from air temperature (Figure 4). Other modeling studies have found similar model deficiencies,
757 for example, Holm et al., (2014) found that the CLM4 was unable to reproduce the range of leaf
758 temperatures observed at a tropical site. Duursma and Medlyn, (2012) found that the MAESPA
759 model was unable to capture the vertical profile of canopy temperatures using a multilayer
760 canopy model. Venturas et al., (2018) compared leaf temperatures of Aspen measured with
761 thermocouples to leaf temperatures simulated with the Gain-Risk model and found the model
762 underestimated midday leaf temperatures (mean absolute leaf temperature error of 1.7°C or
763 5.2%). Biases in leaf temperature influence the calculation of leaf-to-air VPD (used in the
764 calculation of transpiration) and can propagate through photosynthetic and stomatal optimization
765 functions. Furthermore, since leaf metabolic processes depend non-linearly on leaf temperature
766 small biases can manifest into large discrepancies, impacting model performance. When the leaf
767 temperature was prescribed in the MED-H model using the observed canopy temperature, the
768 cumulative growing season mean transpiration was 5% higher. The increased morning
769 transpiration and decreased afternoon transpiration better matched the observed diurnal pattern
770 of sapflow measurements (Figure 5).

771
772 These findings emphasize the need to address model deficiencies in the representation of canopy
773 temperature. Big-leaf models have deficiencies in capturing canopy temperatures since the whole
774 canopy experiences equivalent air temperatures. Multilayer canopy models can capture the
775 vertical profiles of radiation and within-canopy air temperatures which studies have found to
776 improve simulated surface fluxes (Chen et al., 2016; Bonan et al., 2018). In the SPA multilayer
777 canopy model, the above-canopy temperature is applied at all canopy layers, assuming within-
778 canopy air is well-mixed. Bonan et al., (2021) demonstrated that using uniform vertical profiles

779 of air temperatures in multilayer canopy models results in nearly identical fluxes as big-leaf
780 models. When the well-mixed assumption is removed and the vertical profile of air temperatures
781 are resolved, Bonan et al., (2021) showed considerable improvement in canopy fluxes. This
782 suggests that a first step toward addressing canopy temperature biases in multilayer models
783 would be to resolve vertical air temperature profiles. A second step would be to examine the role
784 of leaf boundary layer processes, which also likely contribute to leaf temperature biases. Finally,
785 the accuracy of the radiation transfer scheme should be assessed, which requires within canopy
786 observational data.

787

788 *4.3 Water-use efficiency*

789

790 Stable carbon isotopes have long been used to provide information on plant water use efficiency
791 (Farquhar & Richards 1984; Farquhar et al., 1989; Condon, Richards & Farquhar 1993). The
792 dynamics of isotopic discrimination can be used to evaluate how ecosystem models respond to
793 environmental drivers on interannual timescales (Lavergne et al., 2019; 2020a; 2020b). Here we
794 illustrated the value of $\Delta^{13}\text{C}$ observations for discerning model behavior. The Gain-Risk model
795 simulates the strongest reduction in monthly mean $\Delta^{13}\text{C}$ in response to reduced canopy water
796 potential (Figure 7). This is because the Gain-Risk model varies the water use efficiency
797 optimally to maximize carbon gain while avoiding loss of hydraulic function. The WUEi model
798 maintains near constant $\Delta^{13}\text{C}$ until the minimum canopy water potential (-2 MPa) is reached. The
799 stomatal efficiency parameter defines the marginal water cost of carbon that constrains the
800 intrinsic water use efficiency ($\Delta A/\Delta g_s$) and thus the $\Delta^{13}\text{C}$. In the WUE model the stomatal
801 efficiency parameter defines the instantaneous water use efficiency ($\Delta A/\Delta T$) and thus modifies
802 the water use efficiency in response to VPD. Therefore, the decline in $\Delta^{13}\text{C}$ with reduced canopy
803 water potential simulated by the WUE model is likely attributable to the correlation between
804 VPD and canopy water potential.

805

806 The BB-H and MED-H models originally used a fixed water-use efficiency, defined by the g_l
807 parameter. Here we implemented a hydraulic stress constraint which modifies the g_l parameter in
808 response to canopy water potential (eq. 5). The result is a linear reduction in $\Delta^{13}\text{C}$ with reduced
809 canopy water potential (Figure 7). Kennedy et al., (2019) implemented a similar constraint in the

810 CLM5 model but applied the hydraulic limitation by modifying V_{cmax} . Whether drought stress
811 affects the water-use efficiency of plants or acts directly on photosynthetic capacity is still an
812 open question. Zhou et al., (2013) found that downregulation of the g_1 parameter was insufficient
813 to account for observed changes in GPP in response to water limitation, and thus modification of
814 V_{cmax} was required. However, Lin et al., (2018) suggest that the g_1 parameter is not sensitive to
815 water limitations and only the intercept, g_0 , and GPP are sensitive to soil water availability.

816

817 Observations of $\Delta^{13}C$ would be a valuable tool for better understanding the effects of drought
818 stress on plant gas exchange and may elucidate differences in model representations of hydraulic
819 functioning. The National Ecological Observatory Network (NEON) measures atmospheric CO_2
820 isotope ratios across ecosystems at high temporal frequencies (Fiorella et al., 2021). We suggest
821 that this observational network could serve as a valuable model testbed and encourage future
822 cross-site model evaluation studies.

823

824 *4.4 Information flows*

825

826 We took an information theoretical approach to decompose multi-variate mutual information
827 between transpiration and its key drivers to assess process representation in models
828 independently of parametric assumptions. Similarly to Bassiouni & Vico, (2021), we found that
829 all models had high overall functional performance (Figure 9). Generally, the more empirical
830 models (BB-H & MED-H) had better functional performance when soil water was not limiting
831 (Figure S6) while models with more mechanistic representations of hydraulic functioning
832 (WUEi, WUE, Gain-Risk) had better functional performance when soil water availability was
833 low (Figure 9). It is common for more empirical, multiplicative models (such as MED-H) to
834 better represent synergistic information while more mechanistic additive models (such as Gain-
835 Risk) can underestimate interactions among processes and thus trade synergistic for unique
836 information. This result illustrates how semi-empirical models can compensate for incomplete
837 process representation and capture functional relationships across scales, while incomplete
838 processes in more mechanistic models are more easily discernible. The WUEi and Gain-Risk
839 models had larger tradeoffs between predictive performance and functional accuracy compared
840 to WUE and MED-H, pointing to the possibility that the WUEi and Gain-Risk models accurately

841 estimate the variability in transpiration at the expense of poorer process representations. This
842 finding was clearer from the information metrics than the individual processes diagnostics.

843
844 This study builds upon the work of Bassiouni & Vico, (2021) by implementing stomatal models
845 within multi-layer canopy (and big-leaf) ecosystem models and solving optimization routines
846 numerically. The findings of both studies agree; more mechanistic representations of plant
847 hydraulic functioning did not substantially improve predictive performance or functional
848 accuracy. Our results indicate that semi-empirical models, in particular MED-H, can be
849 effectively adapted to incorporate hydraulic constraints based on measurable plant traits. Model
850 evaluation metrics based on information flows allowed us to go beyond evaluating model
851 performance based on magnitude and seasonality (e.g. Sabot et al., 2020) and examine the causal
852 relationships among the physiological controls on transpiration. The performance metrics also
853 complement the analysis of individual model sensitivities of G_c to VPD and C_i/C_a to P because
854 they help differentiate between effective functional differences and predictive accuracy.
855 However, additional analyses are needed to further interpret the mechanisms driving
856 information-based performance metrics and test whether models with improved functional
857 accuracy perform better under non-stationary climate conditions. We encourage cross-scale
858 model evaluations spanning a range of ecosystems and advocate for the use of information
859 theory to evaluate causal relationships in complex ecological systems.

860

861 **5 Conclusions**

862

863 As the consequences of model representation of stomatal functioning become apparent at large
864 scales (e.g., Kala et al., 2016), much effort has gone into updating the representation of hydraulic
865 functioning in Earth System Models (e.g. Kennedy et al., 2019, Eller et al., 2020, Sabot et al.,
866 2020). To ensure processes are adequately captured across scales, model evaluations must go
867 beyond mean state and variability of leaf-level gas exchange measurements and find new ways to
868 diagnose functional performance and leverage new analytical techniques. Here, we compared a
869 suite of ecosystem models with different representations of hydraulic constraints on stomatal
870 function and identified model specific strengths and deficiencies at a semi-arid ponderosa pine
871 site. We found that models generally performed similarly under unstressed conditions, but

872 performance diverged under atmospheric and soil drought. The more empirical models over
873 estimated synergistic information flows between soil water potential and vapor pressure deficit to
874 transpiration, while the more mechanistic models were overly deterministic.

875

876 This analysis highlights three directions for future ecosystem model development and evaluation:
877 First, it's likely that model structure constrains the flexibility of models to represent a broad
878 spectrum of (an)isohydric behavior. Second, both multilayer canopy and big-leaf models were
879 unable to capture the magnitude of the divergence of canopy temperature from air temperature
880 and given the crucial role of canopy temperature in simulating metabolic processes, diagnosing
881 the causes of model biases should be a priority. Lastly, models diverged in their representation of
882 $\Delta^{13}\text{C}$ under stress thus measurements of stable carbon isotopes may help characterize ecosystem
883 function and elucidate differences attributable to model structure. Future work is needed to
884 explore model structural constraints on ecosystem functional behavior.

885 **Acknowledgments**

886 The authors would like to thank Matt Williams and Luke Smallman for technical support for the
887 SPA model, and Henry Todd for technical support with the Gain-Risk model. This work was
888 funded by the National Science Foundation, Division of Environmental Biology, through the
889 macrosystems biology and NEON-enable science program grant number DEB-1802885. MB
890 received funding from the European Commission and Swedish Research Council for Sustainable
891 Development (FORMAS) (grant 2018-02787) in the frame of the international consortium
892 iAqueduct financed under the 2018 Joint call of the WaterWorks2017 ERA-NET Cofund. MDV
893 was supported by H2020-MSCA-IF-2019 grant No. 882216.

894

895 **Open research**

896 Model code, configuration, and simulations, observational data, and PYTHON scripts required to
897 reproduce this analysis are openly available at <https://zenodo.org/badge/latestdoi/430187802>

898

899 **References**

- 900 Anderegg, W. R. L., Wolf, A., Arango-Velez, A., Choat, B., Chmura, D. J., Jansen, S., Kolb, T.,
901 Li, S., Meinzer, F. C., Pita, P., Resco de Dios, V., Sperry, J. S., Wolfe, B. T., & Pacala, S.
902 (2018). Woody plants optimise stomatal behaviour relative to hydraulic risk. *Ecology*
903 *Letters*, 21(7), 968–977. <https://doi.org/10.1111/ele.12962>
- 904 Aphalo, P. J., & Jarvis, P. G. (1991). Do stomata respond to relative humidity? *Plant, Cell &*
905 *Environment*, 14(1), 127–132. <https://doi.org/10.1111/j.1365-3040.1991.tb01379.x>
- 906 Ball, J. T., Woodrow, I. E., & Berry, J. A. (1987). A Model Predicting Stomatal Conductance
907 and its Contribution to the Control of Photosynthesis under Different Environmental
908 Conditions. In J. Biggins (Ed.), *Progress in Photosynthesis Research: Volume 4*
909 *Proceedings of the VIIth International Congress on Photosynthesis Providence, Rhode*
910 *Island, USA, August 10–15, 1986* (pp. 221–224). Springer Netherlands.
911 https://doi.org/10.1007/978-94-017-0519-6_48
- 912 Bassiouni, M., & Vico, G. (2021). Parsimony vs predictive and functional performance of three
913 stomatal optimization principles in a big-leaf framework. *New Phytologist*, 231(2), 586–
914 600. <https://doi.org/10.1111/nph.17392>
- 915 Bonan, G. B. (1995). Land-atmosphere CO₂ exchange simulated by a land surface process
916 model coupled to an atmospheric general circulation model. *Journal of Geophysical*
917 *Research: Atmospheres*, 100(D2), 2817–2831. <https://doi.org/10.1029/94JD02961>
- 918 Bonan, G. B., Patton, E. G., Finnigan, J. J., Baldocchi, D. D., & Harman, I. N. (2021). Moving
919 beyond the incorrect but useful paradigm: Reevaluating big-leaf and multilayer plant
920 canopies to model biosphere-atmosphere fluxes – a review. *Agricultural and Forest*
921 *Meteorology*, 306, 108435. <https://doi.org/10.1016/j.agrformet.2021.108435>
- 922 Bonan, G. B., Patton, E. G., Harman, I. N., Oleson, K. W., Finnigan, J. J., Lu, Y., & Burakowski,
923 E. A. (2018). Modeling canopy-induced turbulence in the Earth system: A unified
924 parameterization of turbulent exchange within plant canopies and the roughness sublayer
925 (CLM-ml v0). *Geoscientific Model Development*, 11(4), 1467–1496.
926 <https://doi.org/10.5194/gmd-11-1467-2018>
- 927 Bonan, G. B., Williams, M., Fisher, R. A., & Oleson, K. W. (2014). Modeling stomatal
928 conductance in the earth system: Linking leaf water-use efficiency and water transport
929 along the soil–plant–atmosphere continuum. *Geoscientific Model Development*, 7(5),
930 2193–2222. <https://doi.org/10.5194/gmd-7-2193-2014>

- 931 Bowling, D. R., McDowell, N. G., Bond, B. J., Law, B. E., & Ehleringer, J. R. (2002). ¹³C
932 content of ecosystem respiration is linked to precipitation and vapor pressure deficit.
933 *Oecologia*, 131(1), 113–124. <https://doi.org/10.1007/s00442-001-0851-y>
- 934 Buckley, T. N. (2005). The control of stomata by water balance. *New Phytologist*, 168(2), 275–
935 292. <https://doi.org/10.1111/j.1469-8137.2005.01543.x>
- 936 Buckley, T. N. (2017). Modeling Stomatal Conductance. *Plant Physiology*, 174(2), 572–582.
937 <https://doi.org/10.1104/pp.16.01772>
- 938 Buckley, T. N. (2019). How do stomata respond to water status? *New Phytologist*, 224(1), 21–
939 36. <https://doi.org/10.1111/nph.15899>
- 940 Fiorella, R. P., Good, S. P., Allen, S. T., Guo, J. S., Still, C. J., Noone, D. C., Anderegg, W.R.,
941 Florian, C.R., Luo, H., Pingintha-Durden, N. & Bowen, G. J. (2021). Calibration
942 Strategies for Detecting Macroscale Patterns in NEON Atmospheric Carbon Isotope
943 Observations. *Journal of Geophysical Research: Biogeosciences*, 126(3),
944 e2020JG005862.
- 945 Chen, Y., Ryder, J., Bastrikov, V., McGrath, M. J., Naudts, K., Otto, J., Ottlé, C., Peylin, P.,
946 Polcher, J., Valade, A., Black, A., Elbers, J. A., Moors, E., Foken, T., van Gorsel, E.,
947 Haverd, V., Heinesch, B., Tiedemann, F., Knohl, A., ... Luysaert, S. (2016). Evaluating
948 the performance of land surface model ORCHIDEE-CAN v1.0 on water and energy flux
949 estimation with a single- and multi-layer energy budget scheme. *Geoscientific Model
950 Development*, 9(9), 2951–2972. <https://doi.org/10.5194/gmd-9-2951-2016>
- 951 Condon, A. G., Richards, R. A., & Farquhar, G. D. (1993). Relationships between carbon isotope
952 discrimination, water use efficiency and transpiration efficiency for dryland wheat.
953 *Australian Journal of Agricultural Research*, 44(8), 1693–1711.
954 <https://doi.org/10.1071/ar9931693>
- 955 Cover T.M., & Thomas J. A., (2012). Elements of information theory. New York, NY, USA:
956 John Wiley & Sons.
- 957 Cowan, I. R., & Farquhar, G. D. (1977). Stomatal function in relation to leaf metabolism and
958 environment. *Integration of Activity in the Higher Plant*, Cambridge University Press,
959 Cambridge, 471–505. <https://pubmed.ncbi.nlm.nih.gov/756635/>

- 960 Cox, P. M., Huntingford, C., & Harding, R. J. (1998). A canopy conductance and photosynthesis
961 model for use in a GCM land surface scheme. *Journal of Hydrology*, 212–213, 79–94.
962 [https://doi.org/10.1016/S0022-1694\(98\)00203-0](https://doi.org/10.1016/S0022-1694(98)00203-0)
- 963 Damour, G., Simonneau, T., Cochard, H., & Urban, L. (2010). An overview of models of
964 stomatal conductance at the leaf level. *Plant, Cell & Environment*, 33(9), 1419–1438.
965 <https://doi.org/10.1111/j.1365-3040.2010.02181.x>
- 966 Domec, J.-C., Warren, J. M., Meinzer, F. C., Brooks, J. R., & Coulombe, R. (2004). Native root
967 xylem embolism and stomatal closure in stands of Douglas-fir and ponderosa pine:
968 Mitigation by hydraulic redistribution. *Oecologia*, 141(1), 7–16.
969 <https://doi.org/10.1007/s00442-004-1621-4>
- 970 Duursma, R. A., & Medlyn, B. E. (2012). MAESPA: A model to study interactions between
971 water limitation, environmental drivers and vegetation function at tree and stand levels,
972 with an example application to [CO₂] × drought interactions. *Geoscientific Model
973 Development*, 5(4), 919–940. <https://doi.org/10.5194/gmd-5-919-2012>
- 974 Eller, C. B., Rowland, L., Mencuccini, M., Rosas, T., Williams, K., Harper, A., Medlyn, B. E.,
975 Wagner, Y., Klein, T., Teodoro, G. S., Oliveira, R. S., Matos, I. S., Rosado, B. H. P.,
976 Fuchs, K., Wohlfahrt, G., Montagnani, L., Meir, P., Sitch, S., & Cox, P. M. (2020).
977 Stomatal optimization based on xylem hydraulics (SOX) improves land surface model
978 simulation of vegetation responses to climate. *New Phytologist*, 226(6), 1622–1637.
979 <https://doi.org/10.1111/nph.16419>
- 980 Evans, J. R., & Von Caemmerer, S. (2013). Temperature response of carbon isotope
981 discrimination and mesophyll conductance in tobacco. *Plant, Cell & Environment*, 36(4),
982 745–756. <https://doi.org/10.1111/j.1365-3040.2012.02591.x>
- 983 Farquhar, G. D., von Caemmerer, S., & Berry, J. A. (1980). A biochemical model of
984 photosynthetic CO₂ assimilation in leaves of C₃ species. *Planta*, 149, 78–90.
- 985 Farquhar, G. D., O’Leary, M. H., & Berry, J. A. (1982). On the Relationship Between Carbon
986 Isotope Discrimination and the Intercellular Carbon Dioxide Concentration in Leaves.
987 *Functional Plant Biology*, 9(2), 121–137. <https://doi.org/10.1071/pp9820121>
- 988 Farquhar, G. D., & von Caemmerer, S. (1982). Modelling of Photosynthetic Response to
989 Environmental Conditions. In O. L. Lange, P. S. Nobel, C. B. Osmond, & H. Ziegler

- 990 (Eds.), *Physiological Plant Ecology II: Water Relations and Carbon Assimilation* (pp.
991 549–587). Springer. https://doi.org/10.1007/978-3-642-68150-9_17
- 992 Farquhar, G. D., & Richards, R. A. (1984). Isotopic Composition of Plant Carbon Correlates
993 With Water-Use Efficiency of Wheat Genotypes. *Functional Plant Biology*, 11(6), 539–
994 552. <https://doi.org/10.1071/pp9840539>
- 995 Farquhar, G. D., Ehleringer, J. R., & Hubick, K. T. (1989) Carbon isotope discrimination and
996 photosynthesis. *Annual Review Plant Physiology Plant Molecular Biology* 40, 503–537.
- 997 Feng, X. (1999). Trends in intrinsic water-use efficiency of natural trees for the past 100–200
998 years: a response to atmospheric CO₂ concentration. *Geochimica et Cosmochimica Acta*,
999 63(13-14), 1891-1903.
- 1000 Fiorella, R. P., Good, S. P., Allen, S. T., Guo, J. S., Still, C. J., Noone, D. C., Anderegg, W. R.
1001 L., Florian, C. R., Luo, H., Pingingtha-Durden, N., & Bowen, G. J. (2021). Calibration
1002 Strategies for Detecting Macroscale Patterns in NEON Atmospheric Carbon Isotope
1003 Observations. *Journal of Geophysical Research: Biogeosciences*, 126(3),
1004 e2020JG005862. <https://doi.org/10.1029/2020JG005862>
- 1005 Fisher, R. A., Williams, M., Do Vale, R. L., Da Costa, A. L., & Meir, P. (2006). Evidence from
1006 Amazonian forests is consistent with isohydric control of leaf water potential. *Plant, Cell
1007 & Environment*, 29(2), 151–165. <https://doi.org/10.1111/j.1365-3040.2005.01407.x>
- 1008 Franks, P. J., Berry, J. A., Lombardozzi, D. L., & Bonan, G. B. (2017). Stomatal Function across
1009 Temporal and Spatial Scales: Deep-Time Trends, Land-Atmosphere Coupling and Global
1010 Models. *Plant Physiology*, 174(2), 583–602. <https://doi.org/10.1104/pp.17.00287>
- 1011 Goodwell, A. E., Jiang, P., Ruddell, B. L., & Kumar, P. (2020). Debates—Does Information
1012 Theory Provide a New Paradigm for Earth Science? Causality, Interaction, and Feedback.
1013 *Water Resources Research*, 56(2), e2019WR024940.
1014 <https://doi.org/10.1029/2019WR024940>
- 1015 Goodwell, A. E., & Kumar, P. (2017). Temporal information partitioning: Characterizing
1016 synergy, uniqueness, and redundancy in interacting environmental variables. *Water
1017 Resources Research*, 53(7), 5920–5942. <https://doi.org/10.1002/2016WR020216>
- 1018 Granier, A. (1987). Evaluation of transpiration in a Douglas-fir stand by means of sap flow
1019 measurements. *Tree Physiology*, 3(4), 309–320. <https://doi.org/10.1093/treephys/3.4.309>

- 1020 Hill, T. C., Williams, M., & Moncrieff, J. B. (2008). Modeling feedbacks between a boreal forest
1021 and the planetary boundary layer. *Journal of Geophysical Research: Atmospheres*,
1022 *113*(D15). <https://doi.org/10.1029/2007JD009412>
- 1023 Holm, J. A., Jardine, K., Guenther, A. B., Chambers, J. Q., & Tribuzy, E. (2014). Evaluation of
1024 MEGAN-CLM parameter sensitivity to predictions of isoprene emissions from an
1025 Amazonian rainforest. *Atmospheric Chemistry and Physics Discussions*, *14*(17), 23995–
1026 24041. <https://doi.org/10.5194/acpd-14-23995-2014>
- 1027 Irvine, J., Law, B. E., Kurpius, M. R., Anthoni, P. M., Moore, D., & Schwarz, P. A. (2004). Age-
1028 related changes in ecosystem structure and function and effects on water and carbon
1029 exchange in ponderosa pine. *Tree Physiology*, *24*(7), 753–763.
1030 <https://doi.org/10.1093/treephys/24.7.753>
- 1031 Irvine, J., Law, B. E., Martin, J. G., & Vickers, D. (2008). Interannual variation in soil CO₂
1032 efflux and the response of root respiration to climate and canopy gas exchange in mature
1033 ponderosa pine. *Global Change Biology*, *14*(12), 2848–2859.
1034 <https://doi.org/10.1111/j.1365-2486.2008.01682.x>
- 1035 Johnson, D. M., Woodruff, D. R., McCulloh, K. A., & Meinzer, F. C. (2009). Leaf hydraulic
1036 conductance, measured in situ, declines and recovers daily: Leaf hydraulics, water
1037 potential and stomatal conductance in four temperate and three tropical tree species. *Tree*
1038 *Physiology*, *29*(7), 879–887. <https://doi.org/10.1093/treephys/tpp031>
- 1039 Jones, H. G., & Jones, H. G. (1992). *Plants and Microclimate: A Quantitative Approach to*
1040 *Environmental Plant Physiology*. Cambridge University Press.
- 1041 Kala, J., De Kauwe, M. G., Pitman, A. J., Medlyn, B. E., Wang, Y.-P., Lorenz, R., & Perkins-
1042 Kirkpatrick, S. E. (2016). Impact of the representation of stomatal conductance on model
1043 projections of heatwave intensity. *Scientific Reports*, *6*(1), 23418.
1044 <https://doi.org/10.1038/srep23418>
- 1045 Kannenberg, S. A., Guo, J. S., Novick, K. A., Anderegg, W. R. L., Feng, X., Kennedy, D.,
1046 Konings, A. G., Martínez-Vilalta, J., & Matheny, A. M. (2021). Opportunities, challenges
1047 and pitfalls in characterizing plant water-use strategies. *Functional Ecology*, *n/a*(n/a).
1048 <https://doi.org/10.1111/1365-2435.13945>
- 1049 Kennedy, D., Swenson, S., Oleson, K. W., Lawrence, D. M., Fisher, R., Costa, A. C. L. da, &
1050 Gentine, P. (2019). Implementing Plant Hydraulics in the Community Land Model,

- 1051 Version 5. *Journal of Advances in Modeling Earth Systems*, 11(2), 485–513.
1052 <https://doi.org/10.1029/2018MS001500>
- 1053 Kim, Y., Still, C. J., Hanson, C. V., Kwon, H., Greer, B. T., & Law, B. E. (2016). Canopy skin
1054 temperature variations in relation to climate, soil temperature, and carbon flux at a
1055 ponderosa pine forest in central Oregon. *Agricultural and Forest Meteorology*, 226–227,
1056 161–173. <https://doi.org/10.1016/j.agrformet.2016.06.001>
- 1057 Koepke, D. F., & Kolb, T. E. (2013). Species Variation in Water Relations and Xylem
1058 Vulnerability to Cavitation at a Forest-Woodland Ecotone. *Forest Science*, 59(5), 524–
1059 535. <https://doi.org/10.5849/forsci.12-053>
- 1060 Kwon, H., Law, B. E., Thomas, C. K., & Johnson, B. G. (2018). The influence of hydrological
1061 variability on inherent water use efficiency in forests of contrasting composition, age, and
1062 precipitation regimes in the Pacific Northwest. *Agricultural and Forest Meteorology*,
1063 249(C). <https://doi.org/10.1016/j.agrformet.2017.08.006>
- 1064 Lavergne, A., Graven, H., De Kauwe, M. G., Keenan, T. F., Medlyn, B. E., & Prentice, I. C.
1065 (2019). Observed and modelled historical trends in the water-use efficiency of plants and
1066 ecosystems. *Global Change Biology*, 25(7), 2242–2257.
1067 <https://doi.org/10.1111/gcb.14634>
- 1068 Lavergne, A., Sandoval, D., Hare, V. J., Graven, H., & Prentice, I. C. (2020a). Impacts of soil
1069 water stress on the acclimated stomatal limitation of photosynthesis: Insights from stable
1070 carbon isotope data. *Global Change Biology*, 26(12), 7158–7172.
1071 <https://doi.org/10.1111/gcb.15364>
- 1072 Lavergne, A., Voelker, S., Csank, A., Graven, H., de Boer, H. J., Daux, V., Robertson, I.,
1073 Dorado-Liñán, I., Martínez-Sancho, E., Battipaglia, G., Bloomfield, K. J., Still, C. J.,
1074 Meinzer, F. C., Dawson, T. E., Julio Camarero, J., Clisby, R., Fang, Y., Menzel, A.,
1075 Keen, R. M., ... Prentice, I. C. (2020b). Historical changes in the stomatal limitation of
1076 photosynthesis: Empirical support for an optimality principle. *New Phytologist*, 225(6),
1077 2484–2497. <https://doi.org/10.1111/nph.16314>
- 1078 Law, B. E., Cescatti, A., & Baldocchi, D. D. (2001). Leaf area distribution and radiative transfer
1079 in open-canopy forests: Implications for mass and energy exchange. *Tree Physiology*,
1080 21(12–13), 777–787. <https://doi.org/10.1093/treephys/21.12-13.777>

- 1081 Leuning, R. (1995). A critical appraisal of a combined stomatal-photosynthesis model for C3
1082 plants. *Plant, Cell & Environment*, 18(4), 339-355.
- 1083 Li, B., & Good, S. P. (2021). Information-based uncertainty decomposition in dual-channel
1084 microwave remote sensing of soil moisture. *Hydrology and Earth System Sciences*, 25(9),
1085 5029–5045. <https://doi.org/10.5194/hess-25-5029-2021>
- 1086 Lin, C., Gentine, P., Huang, Y., Guan, K., Kimm, H., & Zhou, S. (2018). Diel ecosystem
1087 conductance response to vapor pressure deficit is suboptimal and independent of soil
1088 moisture. *Agricultural and Forest Meteorology*, 250–251, 24–34.
1089 <https://doi.org/10.1016/j.agrformet.2017.12.078>
- 1090 Lin, Y.-S., Medlyn, B. E., Duursma, R. A., Prentice, I. C., Wang, H., Baig, S., Eamus, D., de
1091 Dios, V. R., Mitchell, P., Ellsworth, D. S., de Beeck, M. O., Wallin, G., Uddling, J.,
1092 Tarvainen, L., Linderson, M.-L., Cernusak, L. A., Nippert, J. B., Ocheltree, T. W.,
1093 Tissue, D. T., ... Wingate, L. (2015). Optimal stomatal behaviour around the world.
1094 *Nature Climate Change*, 5(5), 459–464. <https://doi.org/10.1038/nclimate2550>
- 1095 Love, D. M., Venturas, M. D., Sperry, J. S., Brooks, P. D., Pettit, J. L., Wang, Y., Anderegg, W.
1096 R. L., Tai, X., & Mackay, D. S. (2019). Dependence of Aspen Stands on a Subsurface
1097 Water Subsidy: Implications for Climate Change Impacts. *Water Resources Research*,
1098 55(3), 1833–1848. <https://doi.org/10.1029/2018WR023468>
- 1099 McKay, M. D., Beckman, R. J., & Conover, W. J. (1979). A Comparison of Three Methods for
1100 Selecting Values of Input Variables in the Analysis of Output from a Computer Code.
1101 *Technometrics*, 21(2), 239–245. <https://doi.org/10.2307/1268522>
- 1102 Medlyn, B. E., Duursma, R. A., Eamus, D., Ellsworth, D. S., Prentice, I. C., Barton, C. V. M.,
1103 Crous, K. Y., De Angelis, P., Freeman, M., & Wingate, L. (2011). Reconciling the
1104 optimal and empirical approaches to modelling stomatal conductance. *Global Change
1105 Biology*, 17(6), 2134–2144. <https://doi.org/10.1111/j.1365-2486.2010.02375.x>
- 1106 Medlyn, B. E., De Kauwe, M. G., Zaehle, S., Walker, A. P., Duursma, R. A., Luus, K.,
1107 Mishurov, M., Pak, B., Smith, B., Wang, Y.-P., Yang, X., Crous, K. Y., Drake, J. E.,
1108 Gimeno, T. E., Macdonald, C. A., Norby, R. J., Power, S. A., Tjoelker, M. G., &
1109 Ellsworth, D. S. (2016). Using models to guide field experiments: A priori predictions for
1110 the CO2 response of a nutrient- and water-limited native Eucalypt woodland. *Global
1111 Change Biology*, 22(8), 2834–2851. <https://doi.org/10.1111/gcb.13268>

- 1112 Meinzer, F. C., Johnson, D. M., Lachenbruch, B., McCulloh, K. A., & Woodruff, D. R. (2009).
1113 Xylem hydraulic safety margins in woody plants: Coordination of stomatal control of
1114 xylem tension with hydraulic capacitance. *Functional Ecology*, 23(5), 922–930.
1115 <https://doi.org/10.1111/j.1365-2435.2009.01577.x>
- 1116 Mencuccini, M., Manzoni, S., & Christoffersen, B. (2019). Modelling water fluxes in plants:
1117 From tissues to biosphere. *New Phytologist*, 222(3), 1207–1222.
1118 <https://doi.org/10.1111/nph.15681>
- 1119 Misson, L., Panek, J. A., & Goldstein, A. H. (2004). A comparison of three approaches to
1120 modeling leaf gas exchange in annually drought-stressed ponderosa pine forests. *Tree*
1121 *Physiology*, 24(5), 529–541. <https://doi.org/10.1093/treephys/24.5.529>
- 1122 Monteith, J., & Unsworth, M. (1990). *Principles of environmental physics: plants, animals, and*
1123 *the atmosphere*. Academic Press.
- 1124 Novick, K. A., Ficklin, D. L., Stoy, P. C., Williams, C. A., Bohrer, G., Oishi, A. C., Papuga, S.
1125 A., Blanken, P. D., Noormets, A., Sulman, B. N., Scott, R. L., Wang, L., & Phillips, R. P.
1126 (2016). The increasing importance of atmospheric demand for ecosystem water and
1127 carbon fluxes. *Nature Climate Change*, 6(11), 1023–1027.
1128 <https://doi.org/10.1038/nclimate3114>
- 1129 Powell, T. L., Galbraith, D. R., Christoffersen, B. O., Harper, A., Imbuzeiro, H. M. A., Rowland,
1130 L., Almeida, S., Brando, P. M., da Costa, A. C. L., Costa, M. H., Levine, N. M., Malhi,
1131 Y., Saleska, S. R., Sotta, E., Williams, M., Meir, P., & Moorcroft, P. R. (2013).
1132 Confronting model predictions of carbon fluxes with measurements of Amazon forests
1133 subjected to experimental drought. *New Phytologist*, 200(2), 350–365.
1134 <https://doi.org/10.1111/nph.12390>
- 1135 Reinhardt, E., Scott, J., Gray, K., & Keane, R. (2006). Estimating canopy fuel characteristics in
1136 five conifer stands in the western United States using tree and stand measurements.
1137 *Canadian Journal of Forest Research*, 36(11), 2803–2814. [https://doi.org/10.1139/x06-](https://doi.org/10.1139/x06-157)
1138 [157](https://doi.org/10.1139/x06-157)
- 1139 Ruddell, B. L., Drewry, D. T., & Nearing, G. S. (2019). Information Theory for Model
1140 Diagnostics: Structural Error is Indicated by Trade-Off Between Functional and
1141 Predictive Performance. *Water Resources Research*, 55(8), 6534–6554.
1142 <https://doi.org/10.1029/2018WR023692>

- 1143 Ruddell, B. L., & Kumar, P. (2009). Ecohydrologic process networks: 1. Identification. *Water*
1144 *Resources Research*, 45(3). <https://doi.org/10.1029/2008WR007279>
- 1145 Ruehr, N. K., Law, B. E., Quandt, D., & Williams, M. (2014). Effects of heat and drought on
1146 carbon and water dynamics in a regenerating semi-arid pine forest: A combined
1147 experimental and modeling approach. *Biogeosciences*, 11(15), 4139–4156.
1148 <https://doi.org/10.5194/bg-11-4139-2014>
- 1149 Sabot, M. E. B., De Kauwe, M. G., Pitman, A. J., Medlyn, B. E., Verhoef, A., Ukkola, A. M., &
1150 Abramowitz, G. (2020). Plant profit maximization improves predictions of European
1151 forest responses to drought. *New Phytologist*, 226(6), 1638–1655.
1152 <https://doi.org/10.1111/nph.16376>
- 1153 Saltelli, A., & Bolado, R. (1998). An alternative way to compute Fourier amplitude sensitivity
1154 test (FAST). *Computational Statistics & Data Analysis*, 26(4), 445–460.
1155 [https://doi.org/10.1016/S0167-9473\(97\)00043-1](https://doi.org/10.1016/S0167-9473(97)00043-1)
- 1156 Saxton, K. E., Rawls, W. J., Romberger, J. S., & Papendick, R. I. (1986). Estimating Generalized
1157 Soil-water Characteristics from Texture. *Soil Science Society of America Journal*, 50(4),
1158 1031–1036. <https://doi.org/10.2136/sssaj1986.03615995005000040039x>
- 1159 Schwarz, P. A., Law, B. E., Williams, M., Irvine, J., Kurpius, M., & Moore, D. (2004). Climatic
1160 versus biotic constraints on carbon and water fluxes in seasonally drought-affected
1161 ponderosa pine ecosystems. *Global Biogeochemical Cycles*, 18(4).
1162 <https://doi.org/10.1029/2004GB002234>
- 1163 Shannon, C. E. (1948). A mathematical theory of communication. *The Bell System Technical*
1164 *Journal*, 27(3), 379–423. <https://doi.org/10.1002/j.1538-7305.1948.tb01338.x>
- 1165 Smallman, T. L., Moncrieff, J. B., & Williams, M. (2013). WRFv3.2-SPA v2: Development and
1166 validation of a coupled ecosystem–atmosphere model, scaling from surface fluxes of CO₂
1167 and energy to atmospheric profiles. *Geoscientific Model Development*, 6(4), 1079–1093.
1168 <https://doi.org/10.5194/gmd-6-1079-2013>
- 1169 Sperry, J. S., & Love, D. M. (2015). What plant hydraulics can tell us about responses to
1170 climate-change droughts. *New Phytologist*, 207(1), 14–27.
1171 <https://doi.org/10.1111/nph.13354>
- 1172 Sperry, J. S., Venturas, M. D., Anderegg, W. R. L., Mencuccini, M., Mackay, D. S., Wang, Y., &
1173 Love, D. M. (2017). Predicting stomatal responses to the environment from the

- 1174 optimization of photosynthetic gain and hydraulic cost. *Plant, Cell & Environment*,
1175 40(6), 816–830. <https://doi.org/10.1111/pce.12852>
- 1176 Sperry, J. S., Venturas, M. D., Todd, H. N., Trugman, A. T., Anderegg, W. R. L., Wang, Y., &
1177 Tai, X. (2019). The impact of rising CO₂ and acclimation on the response of US forests
1178 to global warming. *Proceedings of the National Academy of Sciences*, 116(51), 25734–
1179 25744. <https://doi.org/10.1073/pnas.1913072116>
- 1180 Sperry, J. S., Wang, Y., Wolfe, B. T., Mackay, D. S., Anderegg, W. R. L., McDowell, N. G., &
1181 Pockman, W. T. (2016). Pragmatic hydraulic theory predicts stomatal responses to
1182 climatic water deficits. *New Phytologist*, 212(3), 577–589.
1183 <https://doi.org/10.1111/nph.14059>
- 1184 Still, C., Powell, R., Aubrecht, D., Kim, Y., Helliker, B., Roberts, D., Richardson, A. D., &
1185 Goulden, M. (2019). Thermal imaging in plant and ecosystem ecology: Applications and
1186 challenges. *Ecosphere*, 10(6), e02768. <https://doi.org/10.1002/ecs2.2768>
- 1187 Stout, D. H., & Sala, A. (2003). Xylem vulnerability to cavitation in *Pseudotsuga menziesii* and
1188 *Pinus ponderosa* from contrasting habitats. *Tree Physiology*.
1189 <https://doi.org/10.1093/TREEPHYS/23.1.43>
- 1190 Sus, O., Poyatos, R., Barba, J., Carvalhais, N., Llorens, P., Williams, M., & Vilalta, J. M. (2014).
1191 Time variable hydraulic parameters improve the performance of a mechanistic stand
1192 transpiration model. A case study of Mediterranean Scots pine sap flow data assimilation.
1193 *Agricultural and Forest Meteorology*, 198–199, 168–180.
1194 <https://doi.org/10.1016/j.agrformet.2014.08.009>
- 1195 Thomas, C. K., Law, B. E., Irvine, J., Martin, J. G., Pettijohn, J. C., & Davis, K. J. (2009).
1196 Seasonal hydrology explains interannual and seasonal variation in carbon and water
1197 exchange in a semiarid mature ponderosa pine forest in central Oregon. *Journal of*
1198 *Geophysical Research: Biogeosciences*, 114(G4). <https://doi.org/10.1029/2009JG001010>
- 1199 Tuzet, A., Perrier, A., & Leuning, R. (2003). A coupled model of stomatal conductance,
1200 photosynthesis and transpiration. *Plant, Cell & Environment*, 26(7), 1097–1116.
1201 <https://doi.org/10.1046/j.1365-3040.2003.01035.x>
- 1202 Ukkola, A. M., Kauwe, M. G. D., Pitman, A. J., Best, M. J., Abramowitz, G., Haverd, V.,
1203 Decker, M., & Haughton, N. (2016). Land surface models systematically overestimate
1204 the intensity, duration and magnitude of seasonal-scale evaporative droughts.

- 1205 *Environmental Research Letters*, 11(10), 104012. <https://doi.org/10.1088/1748->
1206 [9326/11/10/104012](https://doi.org/10.1088/1748-9326/11/10/104012)
- 1207 Ulrich, D. E. M., Still, C., Brooks, J. R., Kim, Y., & Meinzer, F. C. (2019). Investigating old-
1208 growth ponderosa pine physiology using tree-rings, $\delta^{13}\text{C}$, $\delta^{18}\text{O}$, and a process-based
1209 model. *Ecology*, 100(6). <https://doi.org/10.1002/ecy.2656>
- 1210 Venturas, M. D., Sperry, J. S., Love, D. M., Frehner, E. H., Allred, M. G., Wang, Y., &
1211 Anderegg, W. R. L. (2018). A stomatal control model based on optimization of carbon
1212 gain versus hydraulic risk predicts aspen sapling responses to drought. *New Phytologist*,
1213 220(3), 836–850. <https://doi.org/10.1111/nph.15333>
- 1214 Venturas, M. D., Todd, H. N., Trugman, A. T., & Anderegg, W. R. L. (2021). Understanding and
1215 predicting forest mortality in the western United States using long-term forest inventory
1216 data and modeled hydraulic damage. *New Phytologist*, 230(5), 1896–1910.
1217 <https://doi.org/10.1111/nph.17043>
- 1218 Wang, Y., Sperry, J. S., Anderegg, W. R. L., Venturas, M. D., & Trugman, A. T. (2020). A
1219 theoretical and empirical assessment of stomatal optimization modeling. *New*
1220 *Phytologist*, 227(2), 311–325. <https://doi.org/10.1111/nph.16572>
- 1221 Webb, A. (1994). Principles of environmental physics. By J. L. Monteith & M. H. Unsworth.
1222 Edward Arnold, Sevenoaks. 2nd edition, 1990. Pp. Xii + 291. Price £15.99 (£32.00
1223 hardback). ISBN 0 7131 2931 X. *Quarterly Journal of the Royal Meteorological Society*,
1224 120(520), 1700–1700. <https://doi.org/10.1002/qj.49712052015>
- 1225 Williams, M., Rastetter, E. B., Fernandes, D. N., Goulden, M. L., Wofsy, S. C., Shaver, G. R.,
1226 Melillo, J. M., Munger, J. W., Fan, S.-M., & Nadelhoffer, K. J. (1996). Modelling the
1227 soil-plant-atmosphere continuum in a Quercus–Acer stand at Harvard Forest: The
1228 regulation of stomatal conductance by light, nitrogen and soil/plant hydraulic properties.
1229 *Plant, Cell & Environment*, 19(8), 911–927. <https://doi.org/10.1111/j.1365->
1230 [3040.1996.tb00456.x](https://doi.org/10.1111/j.1365-3040.1996.tb00456.x)
- 1231 Williams, M., Law, B. E., Anthoni, P. M., & Unsworth, M. H. (2001a). Use of a simulation
1232 model and ecosystem flux data to examine carbon-water interactions in ponderosa pine.
1233 *Tree Physiology*, 21(5), 287–298. <https://doi.org/10.1093/treephys/21.5.287>
- 1234 Williams, M., Rastetter, E. B., Shaver, G. R., Hobbie, J. E., Carpino, E., & Kwiatkowski, B. L.
1235 (2001b). Primary production of an arctic watershed: an uncertainty analysis. *Ecological*

- 1236 *Applications*, 11(6), 1800–1816. <https://doi.org/10.1890/1051->
1237 [0761\(2001\)011\[1800:PPOAAW\]2.0.CO;2](https://doi.org/10.1890/1051-0761(2001)011[1800:PPOAAW]2.0.CO;2)
- 1238 Williams, M., Schwarz, P. A., Law, B. E., Irvine, J., & Kurpius, M. R. (2005). An improved
1239 analysis of forest carbon dynamics using data assimilation. *Global Change Biology*,
1240 11(1), 89–105. <https://doi.org/10.1111/j.1365-2486.2004.00891.x>
- 1241 Wolf, A., Anderegg, W. R., & Pacala, S. W. (2016). Optimal stomatal behavior with competition
1242 for water and risk of hydraulic impairment. *Proceedings of the National Academy of*
1243 *Sciences*, 113(46), E7222–E7230.
- 1244 Xu, X., Medvigy, D., Powers, J. S., Becknell, J. M., & Guan, K. (2016). Diversity in plant
1245 hydraulic traits explains seasonal and inter-annual variations of vegetation dynamics in
1246 seasonally dry tropical forests. *New Phytologist*, 212(1), 80–95.
1247 <https://doi.org/10.1111/nph.14009>
- 1248 Yang, J., Duursma, R. A., De Kauwe, M. G., Kumarathunge, D., Jiang, M., Mahmud, K.,
1249 Gimeno, T. E., Crous, K. Y., Ellsworth, D. S., Peters, J., Choat, B., Eamus, D., &
1250 Medlyn, B. E. (2019). Incorporating non-stomatal limitation improves the performance of
1251 leaf and canopy models at high vapour pressure deficit. *Tree Physiology*, 39(12), 1961–
1252 1974. <https://doi.org/10.1093/treephys/tpz103>
- 1253 Zhou, S., Duursma, R. A., Medlyn, B. E., Kelly, J. W. G., & Prentice, I. C. (2013). How should
1254 we model plant responses to drought? An analysis of stomatal and non-stomatal
1255 responses to water stress. *Agricultural and Forest Meteorology*, 182–183, 204–214.
1256 <https://doi.org/10.1016/j.agrformet.2013.05.009>